

Supporting Information

Polymorphism of a porous hydrogen bond assisted ionic organic framework

Dániel Vajk Horváth,^a Tamás Holczbauer,^{a,b*} Laura Bereczki,^b Roberta Palkó,^a Nóra Veronika May,^b Tibor Soós^a and Petra Bombicz^b

*E-mail: holczbauer.tamas@tk.mta.hu

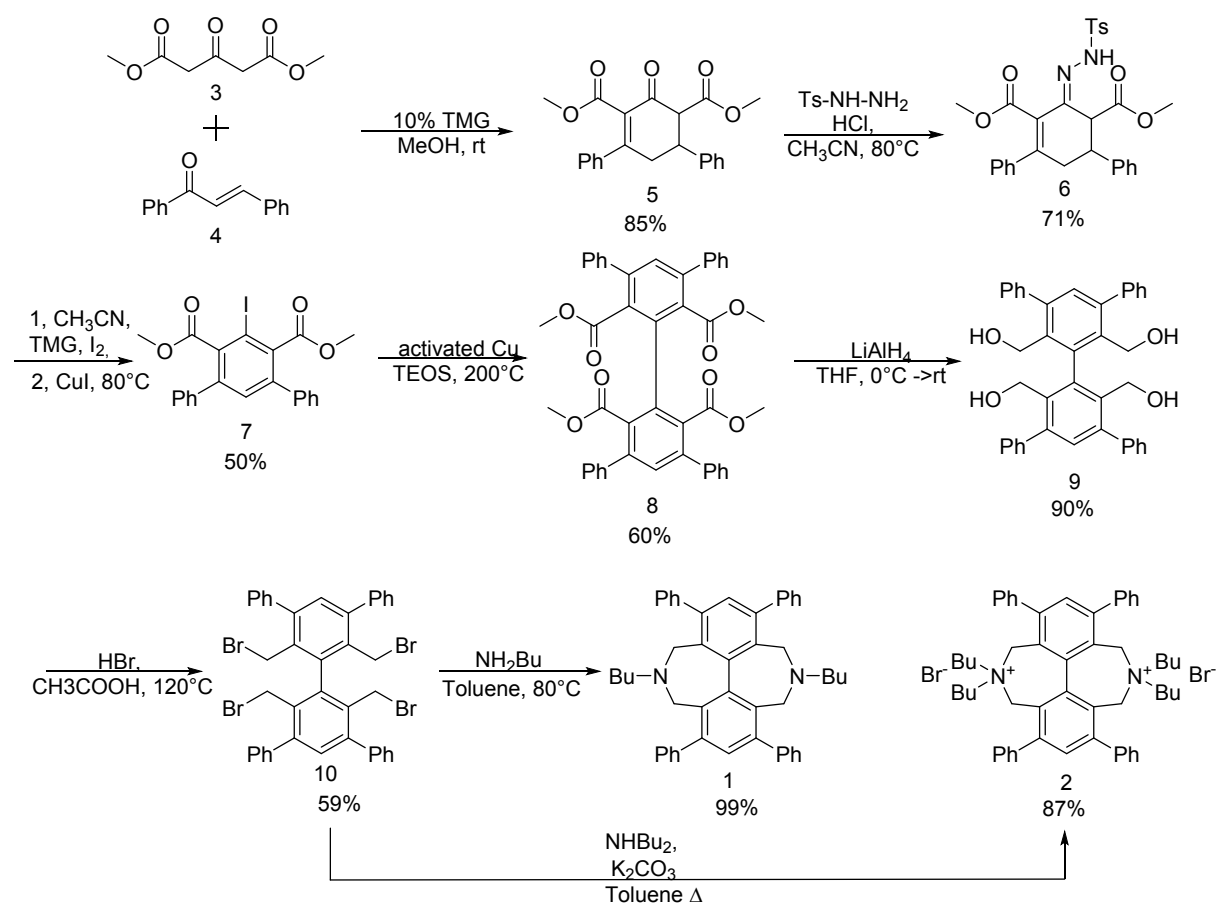
Table of contents

1. Materials and methods	2
1.1 Synthesis	2
1.1.1 General Information about the organic analytical investigations	3
1.1.2 2-oxo-4,6-diphenyl-cyclohex-3-ene-1,3-dicarboxylic acid dimethyl ester (5).....	3
1.1.3 Dimethyl 2-iodo-4,6-diphenylisophthalate (7)	3
1.1.4 3,3',5,5'-tetraphenyl-(1,1'-biphenyl)-2,6,2',6'-tetracarboxylic acid tetramethyl ester (8)	4
1.1.5 2,6,2',6'-tetrakis(hydroxymethyl)-3,5,3',5'-tetraphenyl-1,1'-biphenyl (9).....	5
1.1.6 2,6,2',6'-tetrakis(bromomethyl)-3,5,3',5'-tetraphenyl-biphenyl (10)	5
1.1.7 5,11-dibutyl-1,3,7,9- tetraphenyl - 4,5,6,10,11,12 – hexahydro - 5,11 –diazadibenzo [ef,kl] heptalene (1)	6
1.1.8 5,5-11,11 – tetrabutyl -1,3,7,9 - tetraphenyl - 4,5,6,10,11,12- hexahydro-5,11-diazadibenzo - [ef,kl] heptalene -5,11- diium bromide (2).....	6
1.1.9 5,11- dibutyl - 1,3,7,9 – tetraphenyl - 4,5,6,10,11,12 – hexahydro - 5,11 –diazadibenzo [ef,kl] heptalene dihydrochloride (1c).....	7
1.2 H1-NMR spectra recorded for the synthesized compounds	8
1.3 Growth of the single crystals	16
1.4 Experimental writeup of single crystal structure determination	16
1.5 Generation of Hirshfeld Surfaces	20
2. Structure analysis based on single crystal X-ray diffraction	21
2.1 Discussion of crystal structures of compound 1	21
2.2 Discussion of crystal structures of compound 2	26
2.3 Conformational comparison of compound 1 in crystals 1a-c	32
2.4 Conformational comparison of compound 2 in crystals 2a-c	34
3. Intermolecular interactions investigated by Hirshfeld surface analysis	36
3.1 Hirshfeld surface analysis in structures of compound 1	36
3.2 Hirshfeld surface analysis for crystals of compound 2.....	38

1. Materials and methods

1.1 Synthesis

Compound **1** and **2** were synthesised according to scheme S1.



Scheme S1. Synthesis steps of compound **1** and **2**

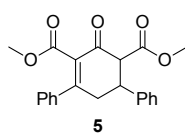
Both (**1**) and (**2**) compounds were synthesised starting from the inexpensive chalcone (**3**) and dimethyl-1,3-acetonedicarboxylate (**4**). The Michael addition and subsequent condensation of dinucleophile (**4**) with dielectrophile (**3**) gave the (**5**) cyclohexanone derivative. This compound was transformed one pot into the (**7**) tetrasubstituted iodobenzene via (**6**) tosylhydrazone intermediate in a Bamford-Stevens type reaction and a following in situ oxidation with 50% yield. The polysubstituted iodo compound (**7**) gave the (**8**) biphenyl in Ullmann homocoupling reaction. The ester function was reduced (**9**) and brominated to give the (**10**) tetrabromo compound. This intermediate was subjected to ring closure with butylamine or dibutylamine to give compound (**1**) (neutral, used to form also the HCl salt) or (**2**) (HBr salt), respectively.

1.1.1 General Information about the organic analytical investigations

Thin layer chromatography (TLC) was performed on Merck Silica gel 60 F₂₅₄ precoated TLC plates (0,25 mm thickness) and visualized with short-wavelength UV light (254 nm). Melting points were recorded on an automatic melting point apparatus (Jasco SRS Optimelt) and are uncorrected. NMR spectra were measured on an 500 MHz instruments at room temperature. Chemical shifts (δ) are reported in ppm relative to residual solvent signals (for ¹H chloroform δ = 7.26 or DMSO δ = 2.50, for ¹³C chloroform δ = 77.00 or DMSO δ = 39.52). Data are reported as follows: chemical shift, multiplicity (s = singlet, d = doublet, t = triplet, q = quartet, m = multiplet), Coupling constants, J, are reported in hertz. High-resolution mass spectra (HRMS) were obtained using an Q-TOF Premier (Waters Corporation).

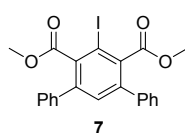
Tetrahydrofuran (THF), toluene were freshly distilled from sodium/benzophenone. All other chemicals were purchased from commercial sources and used as received.

1.1.2 2-oxo-4,6-diphenyl-cyclohex-3-ene-1,3-dicarboxylic acid dimethyl ester (5)



Chalcone (**3**) (8.32 g, 0.04 mol) was dissolved in methanol (40 mL) and dimethyl-1,3-acetonedicarboxylate (**4**) (6 mL, 7.24 g, 0.041 mol, 1.0 eq) was added. The reaction mixture was stirred at room temperature until the chalcone was dissolved. After that 1,1,3,3-tetramethylguanidine (TMG) (2.52 mL, 2.28 g, 0.02 mol, 0.1 eq) was added to the reaction mixture and was refluxed for 3 hours. When the reaction was completed (TLC Hex/EtOAc = 5:1) the reaction mixture was cooled to room temperature, the precipitate was filtered out, and washed with cold methanol. The product was isolated as colourless crystals (12.4 g, 0.034 mol, 85%). M.p.: 160-164 °C. ¹H NMR (CDCl₃) δ 7.33-7.39 (m, 7H), 7.26-7.30 (m, 3H), 3.88 (t, $J_1=5.8$ Hz, $J_2=3.73$ Hz, 2H), 3.64 (s, 3H), 3.59 (s, 3H), 3.03 (d, $J=7.35$ Hz, 2H); ¹³C NMR (CDCl₃) δ 190.2, 168.8, 166.3, 158.7, 140.2, 137.9, 131.9, 130.0, 128.9, 128.7, 127.7, 127.0, 126.6, 59.2, 52.2, 52.1, 43.1, 39.0; HRMS (ESI): m/z [M+Na]⁺ calcd for C₂₂H₂₀NaO₅: 387.1208, found: 387.1216.

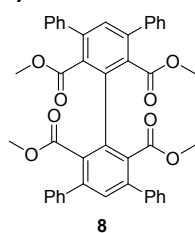
1.1.3 Dimethyl 2-iodo-4,6-diphenylisophthalate (7)



2-oxo-4,6-diphenyl-cyclohex-3-ene-1,3-dicarboxylic acid dimethyl ester (**5**) (12.0 g, 0.032 mol, 1.0 eq) and *p*-toluenesulfonyl hydrazide (6.2 g, 0.0332 mol, 1.04 eq) was dissolved in acetonitrile (380 mL). To the stirred mixture

1.4 mL cc. HCl (0.016 mol, 0.5 eq) was added and it was refluxed for 4 hours. Then *p*-toluenesulfonyl hydrazide (0.96 g, 0.0052 mol, 0.16 eq) was added and the mixture was refluxed for additional 2 hours. It was cooled and TMG (26 mL, 23.94 g, 0.208 mol, 6.5 eq) was added at 0 °C. After 10 minutes of stirring iodine (24.36 g, 0.096 mol, 3.0 eq) was added to the reaction mixture at 0 °C followed by stirring at that temperature for 1 hour. When the reaction was completed (TLC Hex/EtOAc = 3:1) copper iodide (6.7 g, 0.0352 mol, 1.1 eq) was added and the reaction mixture was refluxed for 2 hours, then cooled to room temperature, and was stirred overnight. (Monitoring TLC CH₂Cl₂) The reaction mixture was evaporated to dryness. The residue was dissolved in CH₂Cl₂ (240 mL), the same amount of saturated NaHSO₃ was added and was stirred at room temperature for 15 minutes. The activated charcoal was added to the mixture and was filtered through Celite. The two phases were separated. The organic phase was washed with 10% aq HCl (2 × 100 mL), then sat. NH₃ (3 × 100 mL), then sat. NaCl (2 × 100 mL). The organic phase was dried over Na₂SO₄ and was evaporated to dryness. The residue was recrystallized from methanol and the product was isolated as brown crystals (7.54 g, 0.016 mol, 50%). M.p.: 189-199 °C. ¹H NMR (CDCl₃) δ 7.40 (s, 11H), 3.70 (s, 6H); ¹³C NMR (CDCl₃) δ 168.8, 141.8, 139.4, 138.7, 131.2, 128.4, 128.3, 128.2, 91.2, 52.5; HRMS (ESI): m/z [M+H]⁺ calcd for C₂₂H₁₈IO₄: 473.0250, found: 473.0254.

1.1.4 3,3',5,5'-tetraphenyl-(1,1'-biphenyl)-2,6,2',6'-tetracarboxylic acid tetramethyl ester (8)

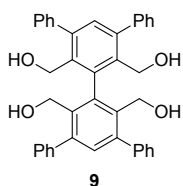


8

Dimethyl 2-iodo-4,6-diphenylisophthalate (7) (7.0 g, 15.0 mmol mol, 1.0 eq), freshly activated copper powder (3.80 g, 59.0 mmol, 4 eq) and tetraethyl-ortosilicate (45 mL) were charged into a Schlenk bomb. Nitrogen was bubbled through the reaction mixture for 10 minutes, then the reaction mixture was heated and kept at 200 °C overnight. (Monitoring TLC CH₂Cl₂)

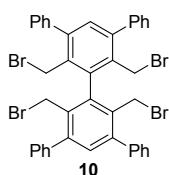
It was cooled down to room temperature, then CH₂Cl₂ (10 mL) was added and it was filtered through Celite pad. The CH₂Cl₂ was distilled off the filtrate, the residue was placed into the refrigerator. The colourless crystals were filtered and were washed with cold methanol and dried to give the title compound as a white solid (3.1 g, 4.5 mmol, 60%). M.p.: 227-233 °C. ¹H NMR (CDCl₃) δ 7.50 (s, 2H), 7.45 (d, *J*=7.17 Hz, 8H), 7.33-7.41 (m, 12H), 3.29 (s, 12H); ¹³C NMR (CDCl₃) δ 167.6, 142.1, 140.4, 136.6, 131.9, 131.3, 128.2 (2), 127.7, 51.5; HRMS (ESI): m/z [M+Na]⁺ calcd for C₄₄H₃₄NaO₈: 713.2151, found: 713.2166.

1.1.5 2,6,2',6'-tetrakis(hydroxymethyl)-3,5,3',5'-tetraphenyl-1,1'-biphenyl (9)



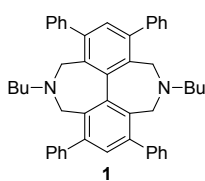
Anhydrous THF (50 mL) was cooled to (-5)-(-10) °C and lithium-aluminium-hydride (1.39 g, 36.0 mmol, 4.1 eq) was added in small portion. Tetramethyl 3,3',5,5'-tetraphenyl-(1,1'-biphenyl)-2,6,2',6'-tetracarboxylic acid tetramethyl ester (8) (6.0 g, 8.6 mmol, 1.0 eq) was dissolved in 65 ml anhydrous THF and was added to the reaction mixture dropwise. The reaction mixture was stirred at (-5)-(-10) °C for 15 minutes, it was allowed to warm to room temperature, and it was stirred at room temperature overnight. (Monitoring TLC CH₂Cl₂) After that the reaction mixture was cooled down to 0 °C, water (1.5 mL) (slowly), 10% NaOH (1.5 mL) and water again (4.5 mL) was added. The reaction mixture was stirred at room temperature for 2 hours. It was filtered through Celite pad with thin silica layer at the bottom and was washed with THF (4 × 15 mL). The filtrate was evaporated to dryness. The product was isolated as colourless crystals (4.49 g, 7.75 mmol, 90%). M.p.: 298-305 °C. ¹H NMR (DMSO) δ 7.89 (d, *J*=7.17 Hz, 8H), 7.38-7.47 (m, 12H), 7.32 (s, 2H), 5.32 (s, 4H), 4.09 (s, 8H); ¹³C NMR (DMSO) δ 142.2, 140.8, 140.5, 135.2, 131.5, 129.4, 127.9, 127.1, 58.6; HRMS (ESI): *m/z* [M+Na]⁺ calcd for C₄₀H₃₄NaO₄: 601.2355, found: 601.2375.

1.1.6 2,6,2',6'-tetrakis(bromomethyl)-3,5,3',5'-tetraphenyl-biphenyl (10)



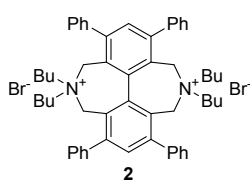
2,6,2',6'-tetrakis(hydroxymethyl)-3,5,3',5'-tetraphenyl-1,1'-biphenyl (9) (4.0 g, 8.4 mmol, 1.0 eq) and 4M HBr in acetic acid (40 mL, 160 mmol, 19.0 eq) was charged into a Schlenk bomb and it was heated to 120 °C and kept for 7 hours. It was cooled to room temperature and stirred overnight. (Monitoring TLC CH₂Cl₂) The reaction mixture was poured to 50 g ice and was extracted with CH₂Cl₂ (2 x 75 mL). Then the organic phase was washed with sat. NaHCO₃ (2 x 50 mL) and brine (1 x 50 mL). The organic phase was dried over Na₂SO₄ and the solvent was evaporated. The product was crystallized from ethyl acetate and was isolated as colourless crystals (4.11 g, 4.95 mmol, 59%). M.p.: 288-295 °C. ¹H NMR (CDCl₃) δ 7.54 (d, *J*=7.17 Hz, 8H), 7.41-7.49 (m, 12H), 7.34 (s, 2H), 4.46 (s, 8H); ¹³C NMR (CDCl₃) δ 144.8, 139.7, 138.3, 133.8, 132.5, 129.0, 128.3, 127.8, 32.4

1.1.7 5,11-dibutyl-1,3,7,9- tetraphenyl - 4,5,6,10,11,12 – hexahydro - 5,11 –diazadibenzo [ef,kl] heptalene (1)



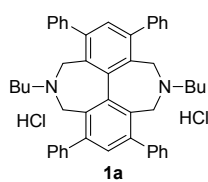
2,6,2',6'-tetrakis(bromomethyl)-3,5,3',5'-tetraphenyl-biphenyl (**10**) (1.038 g, 1.25 mmol, 1.0 eq) and 1-butylamine (1.5 mL, 1.097 g, 15 mmol, 11.5 eq) were dissolved in toluene (40 mL). The reaction mixture was stirred at 80 °C overnight. (Monitoring TLC Hex/EtOAc = 10:1) The reaction mixture was cooled to room temperature, washed with sat. NaHCO₃ solution and the solvent was evaporated to give the title compound as colourless crystals (0.81 g, 1.24 mmol, 99%). M.p.: 221-223 °C. ¹H NMR (CDCl₃) δ 7.60 (d, *J* = 7.13 Hz, 8H), 7.42 (t, *J* = 7.12 Hz, 10H), 7.36 (t, *J* = 7.29 Hz, 4H), 3.90 (d, *J* = 12.37 Hz, 4H), 3.09 (d, *J* = 12.36 Hz, 4H), 2.02-2.13 (m, 4H), 1.09-1.15 (m, 3H), 0.92-1.01 (m, 2H), 0.77-0.83 (m, 2H), 0.73 (t, *J* = 7.3 Hz, 6H); ¹³C NMR (CDCl₃) δ 142.0, 141.3, 140.9, 130.9, 130.8, 130.0, 127.9, 126.9, 54.3, 50.7, 29.5, 20.3, 13.7; HRMS (ESI): *m/z* [M+H]⁺ calcd for C₄₈H₄₉N₂: 653.3896, found: 653.3897.

1.1.8 5,5-11,11 – tetrabutyl -1,3,7,9 - tetraphenyl - 4,5,6,10,11,12- hexahydro-5,11-diazadibenzo - [ef,kl] heptalene -5,11- diium bromide (2)



2,6,2',6'-tetrakis(bromomethyl)-3,5,3',5'-tetraphenyl-biphenyl (**10**) (0.996 g, 1.2 mmol, 1.0 eq), dibutylamine (0.41 mL, 0.310 g, 2.4 mmol, 2.0 eq) and potassium carbonate (0.663 g, 4.8 mmol) were suspended in toluene (20 mL). The reaction mixture was heated for 18 hours. (Monitoring TLC CH₂Cl₂/MeOH = 10:1) It was cooled to room temperature, and the precipitate was filtered, washed with toluene (10 mL), with 2 M aq HBr (2 × 10 mL) and with diethyl - ether (2 × 10 mL). The product was isolated as colourless crystals (0.967 g, 1.04 mmol, 87%). M.p.: 208-213 °C. ¹H NMR (CDCl₃) δ 7.88 (s, 2H), 7.45-7.54 (m, 20H), 4.74 (d, *J* = 13.88 Hz, 4H), 4.54 (d, *J* = 13.74 Hz, 4H), 2.78 (t, *J* = 13.14 Hz, 4H), 2.57 (t, *J* = 12.62 Hz, 4H), 0.79-0.91 (m, 12H), 0.61 (t, *J* = 6.88 Hz, 12H), 0.08 (brs, 3H); ¹³C NMR (CDCl₃) δ 145.3, 143.1, 138.3, 133.0, 131.1, 129.4, 129.3, 129.3, 129.0, 128.8, 128.3, 125.3, 57.1, 57.0, 23.6, 19.5, 13.1; HRMS (ESI): *m/z* [M]²⁺ calcd for C₅₆H₆₆N₂: 766.5226, found: 766.5234.

1.1.9 5,11- dibutyl - 1,3,7,9 - tetraphenyl - 4,5,6,10,11,12 - hexahydro - 5,11 - diazadibenzo [ef,kl] heptalene dihydrochloride (1c)



0.5 g (0.76 mmol, 1.0 eq) 5,11-dibutyl-1,3,7,9-tetraphenyl-4,5,6,10,11,12-hexahydro-5,11-diazadibenzo[ef,kl]heptalene (**1**) was dissolved in THF (10 mL) and 0.8 M HCl in diethyl ether (3 mL, 2.4 mmol, 3.1 eq) was added. The precipitate was filtered and washed with diethyl ether. The

product was isolated as colourless crystals (0.5 g, 0.68 mmol, 90%). M.p.: 226-228 °C. ¹H NMR (CDCl₃) δ 12.98 (brs, 1H), 12.81 (brs, 1H), 7.57-7.40 (m, 17H), 7.35-7.32 (m, 5H), 4.63 (d, *J* = 14.09 Hz, 2H), 4.44 (d, *J* = 10.94 Hz, 2H), 4.20 (d, *J* = 12.15 Hz, 2H), 3.16-3.10 (m, 2H), 2.55-2.45 (m, 4H), 1.69-1.60 (m, 3H), 1.01-0.99 (m, 2H), 0.90-0.82 (m, 3H), 0.65-0.62 (m, 6H); ¹³C NMR (CDCl₃) δ 145.9, 145.73, 145.71, 141.7, 140.6, 139.6, 138.1, 138.0, 137.65, 137.62, 134.6, 133.8, 133.1, 129.3, 129.29, 129.27, 128.7, 128.59, 128.56, 128.4, 126.2, 126.0, 124.7, 124.1, 54.5, 50.2, 47.5, 46.6, 25.7, 19.96, 19.91, 13.0; HRMS (ESI): *m/z* [M+H]⁺ calcd for C₄₈H₄₉N₂: 653.3896, found: 653.3897.

1.2 ¹H-NMR spectra recorded for the synthesized compounds

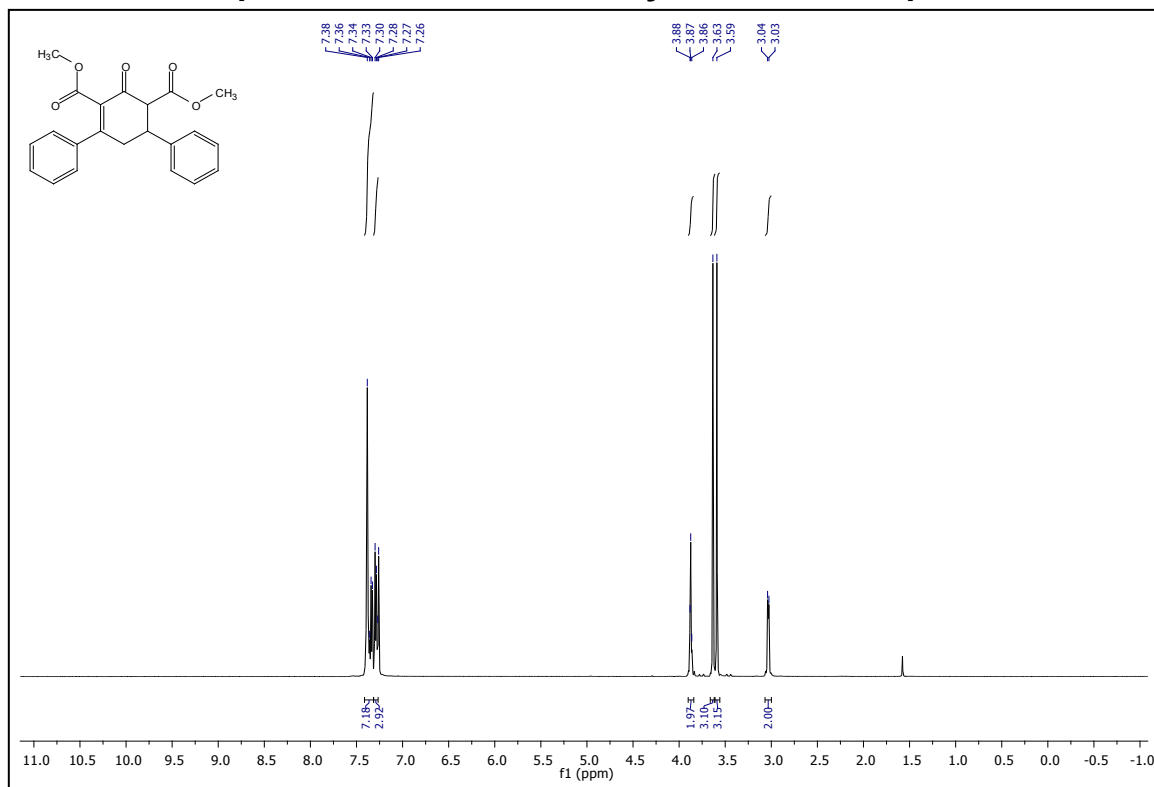


Figure S1. ¹H NMR spectra of **5** at 500 MHz in CDCl₃.

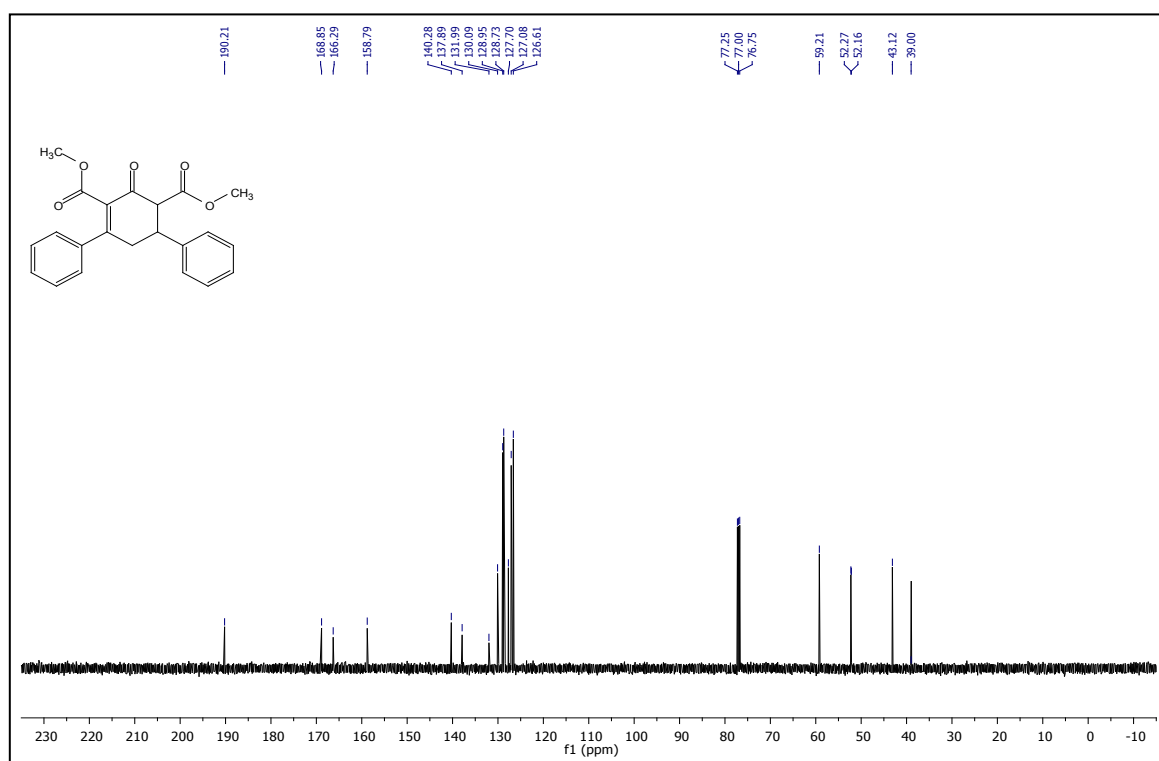


Figure S2. ¹³C NMR spectra of **5** at 125 MHz in CDCl₃.

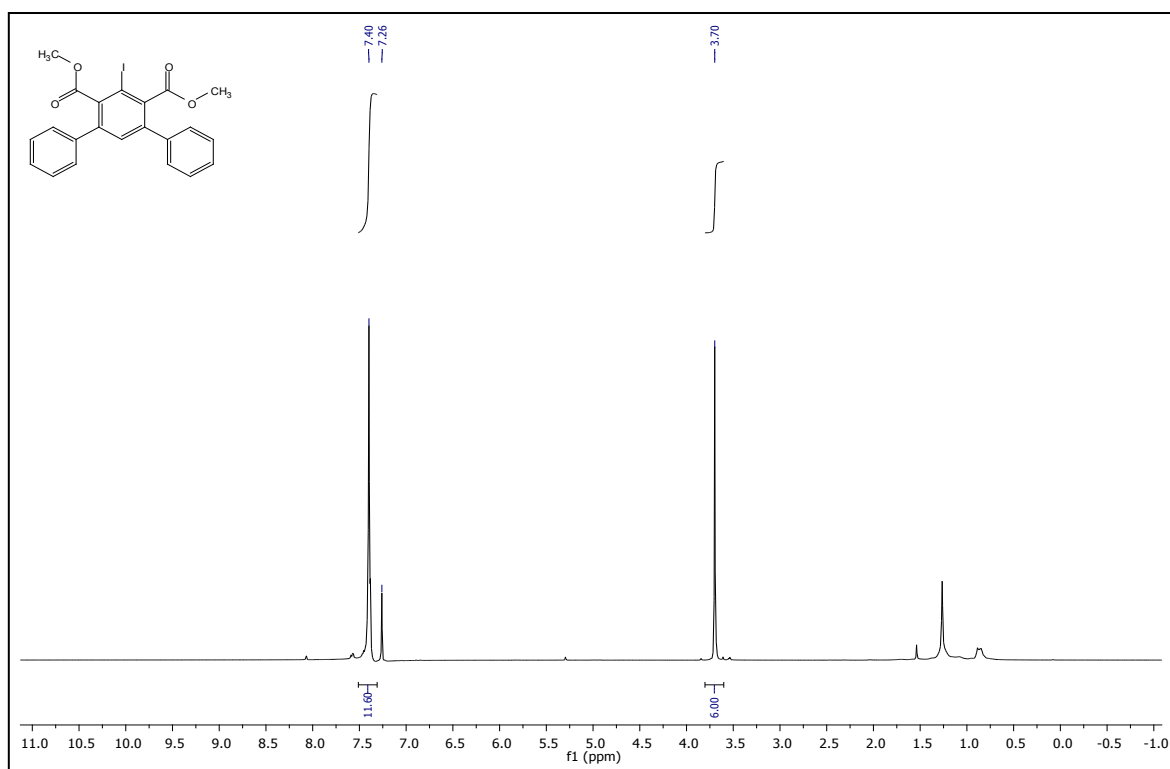


Figure S3. ¹H NMR spectra of 7 at 500 MHz in CDCl₃.

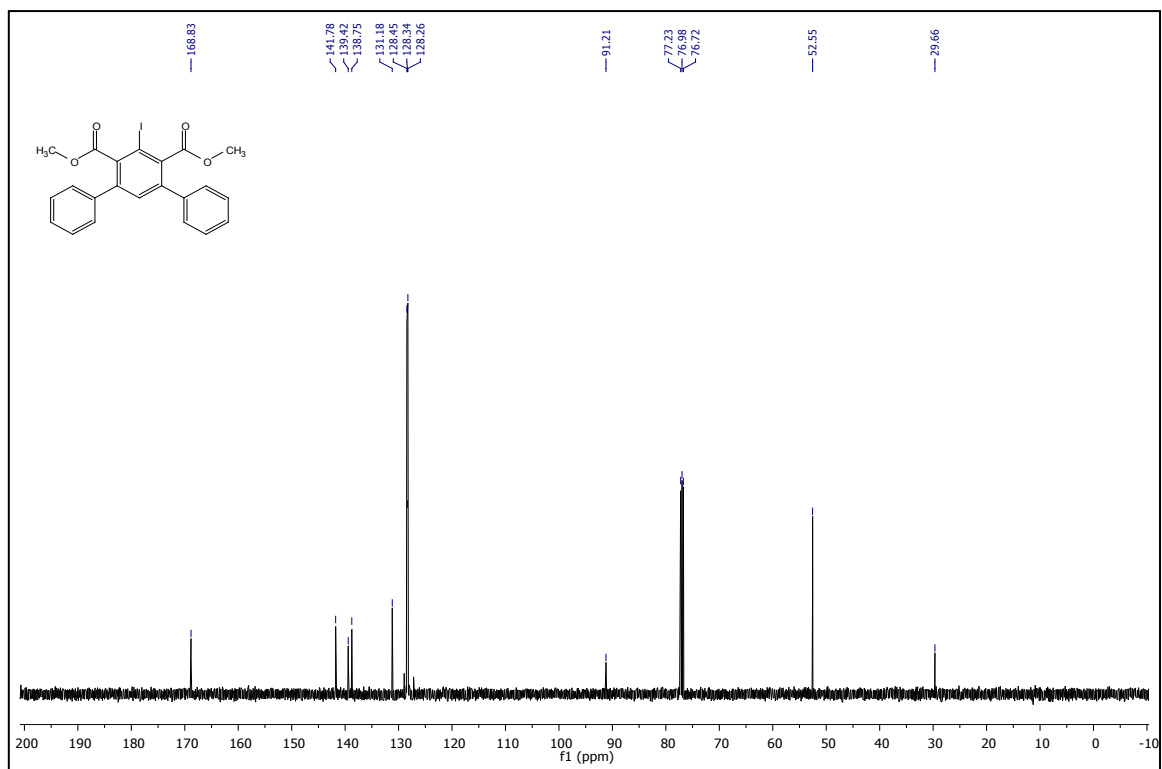


Figure S4. ¹³C NMR spectra of 7 at 125 MHz in CDCl₃.

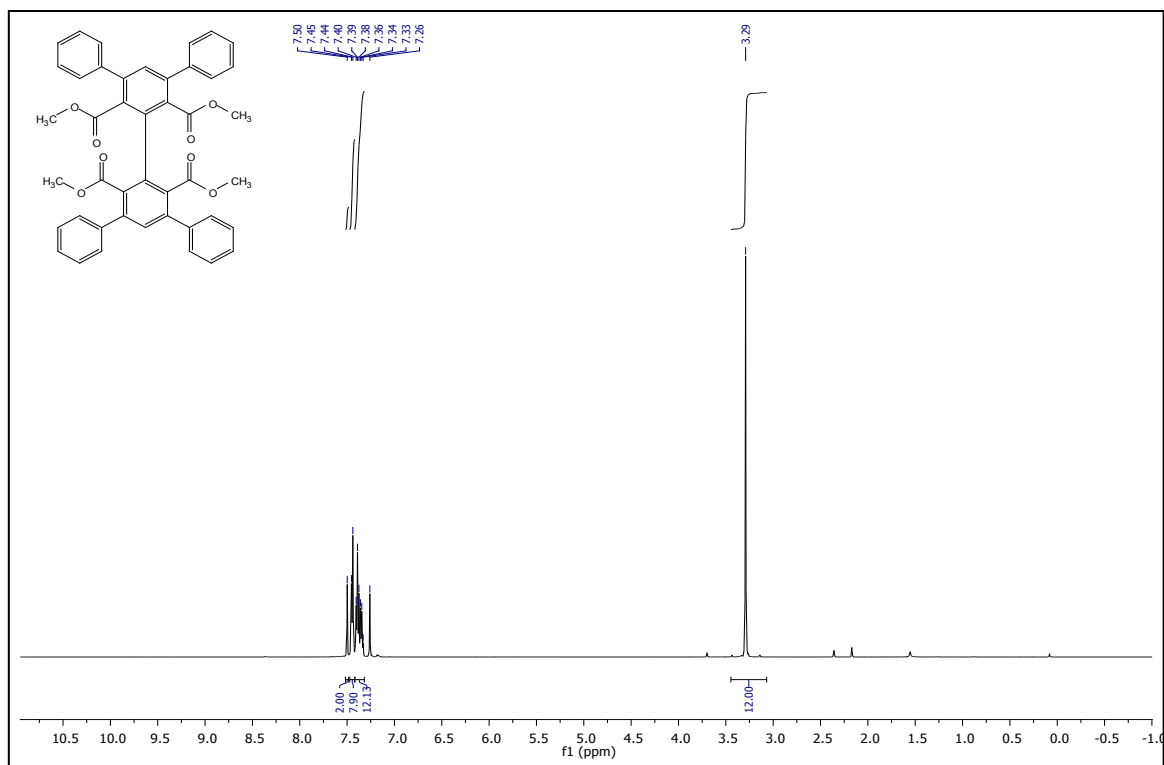


Figure S5. ¹H NMR spectra of **8** at 500 MHz in CDCl₃.

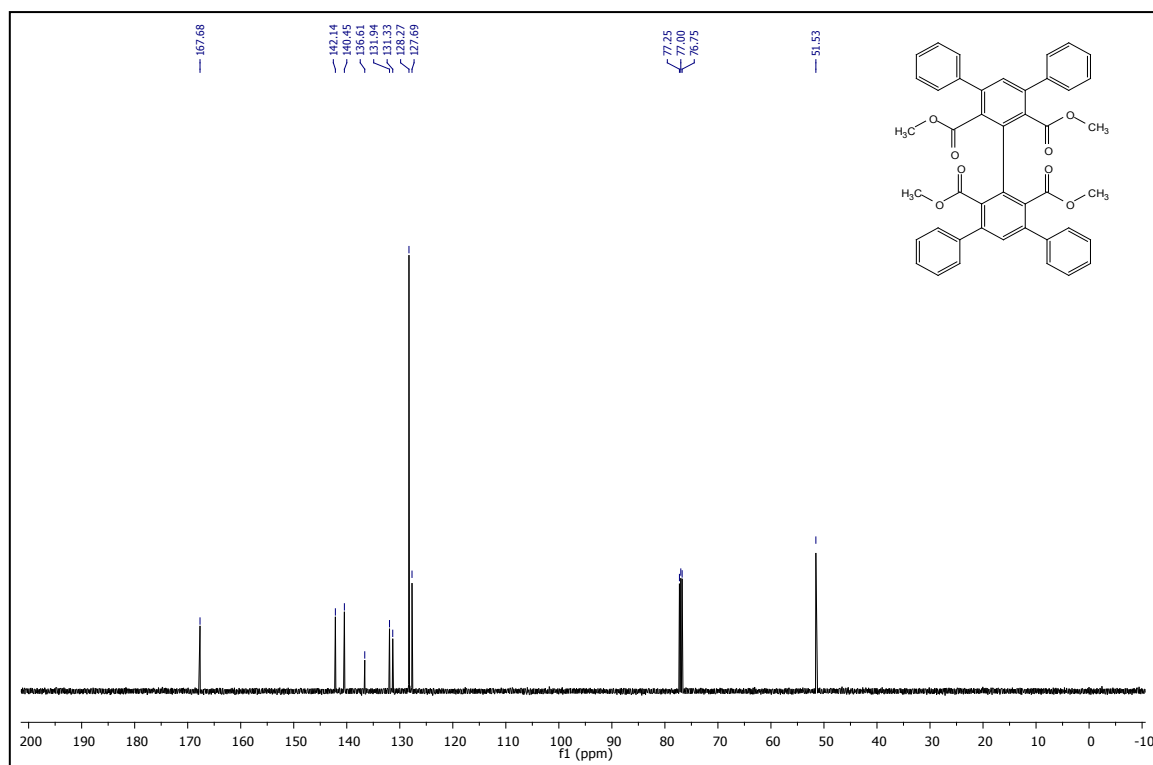


Figure S6. ¹³C NMR spectra of **8** at 125 MHz in CDCl₃.

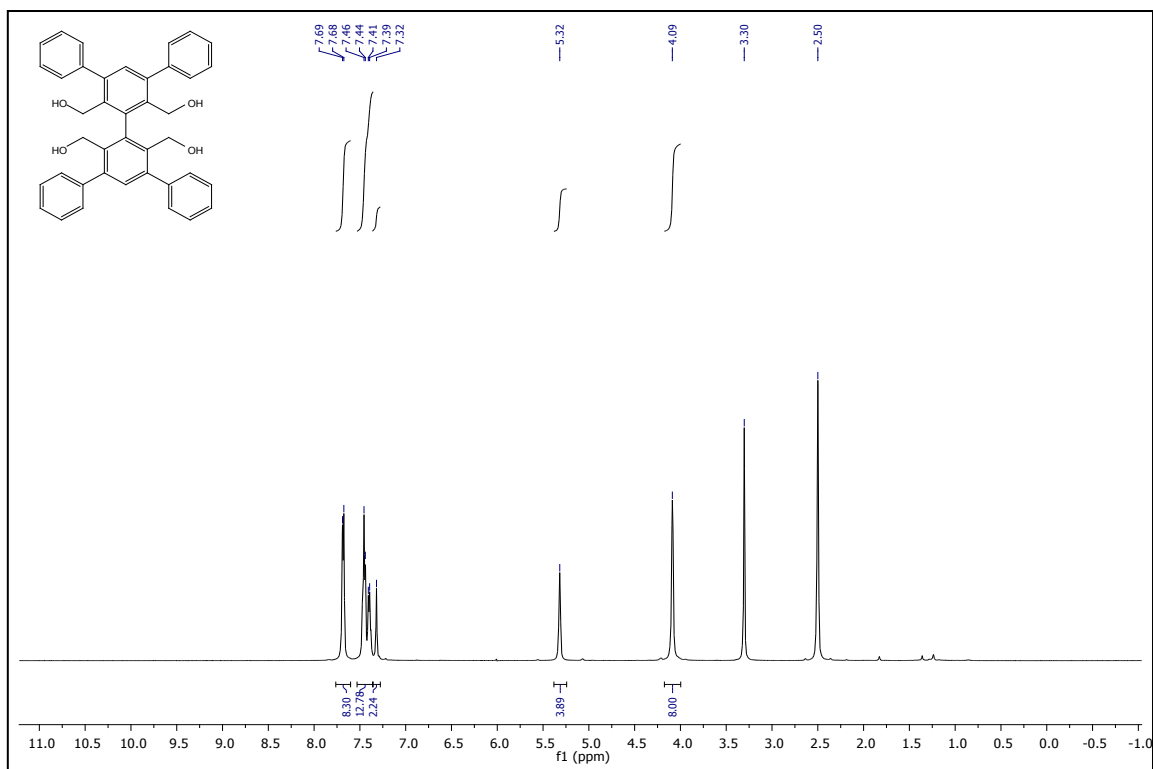


Figure S7. ^1H NMR spectra of **9** at 500 MHz in DMSO.

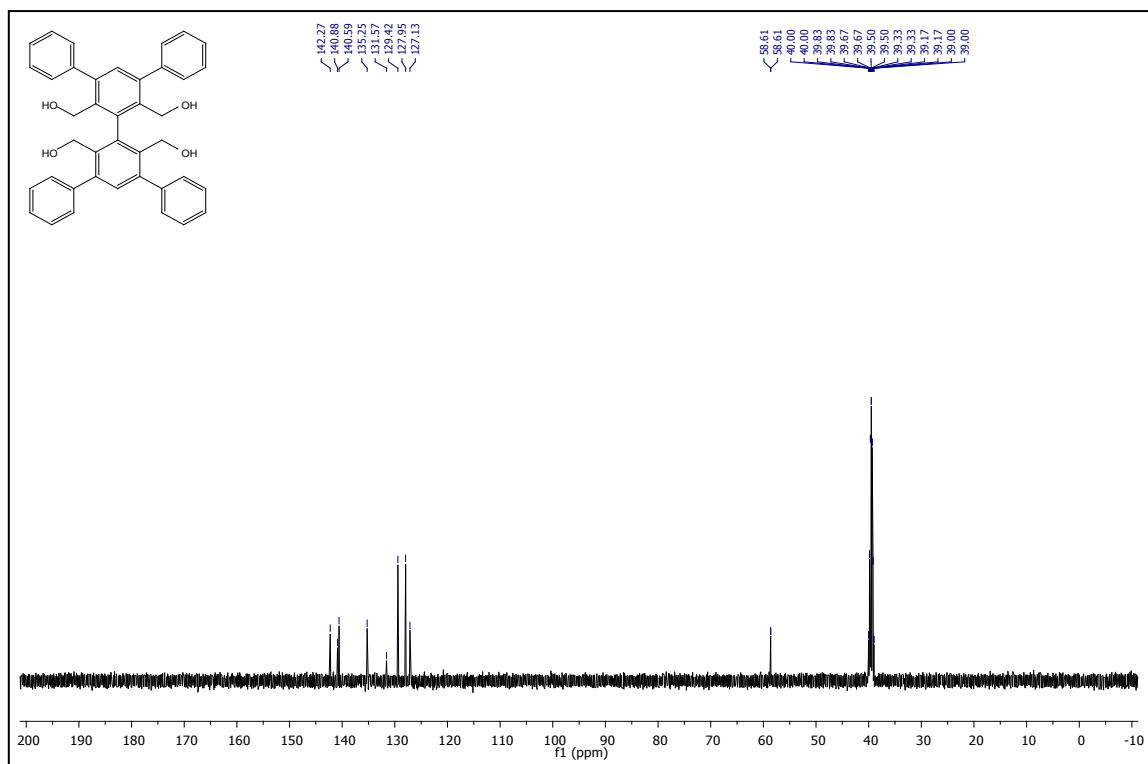


Figure S8. ^{13}C NMR spectra of **9** at 125 MHz in DMSO.

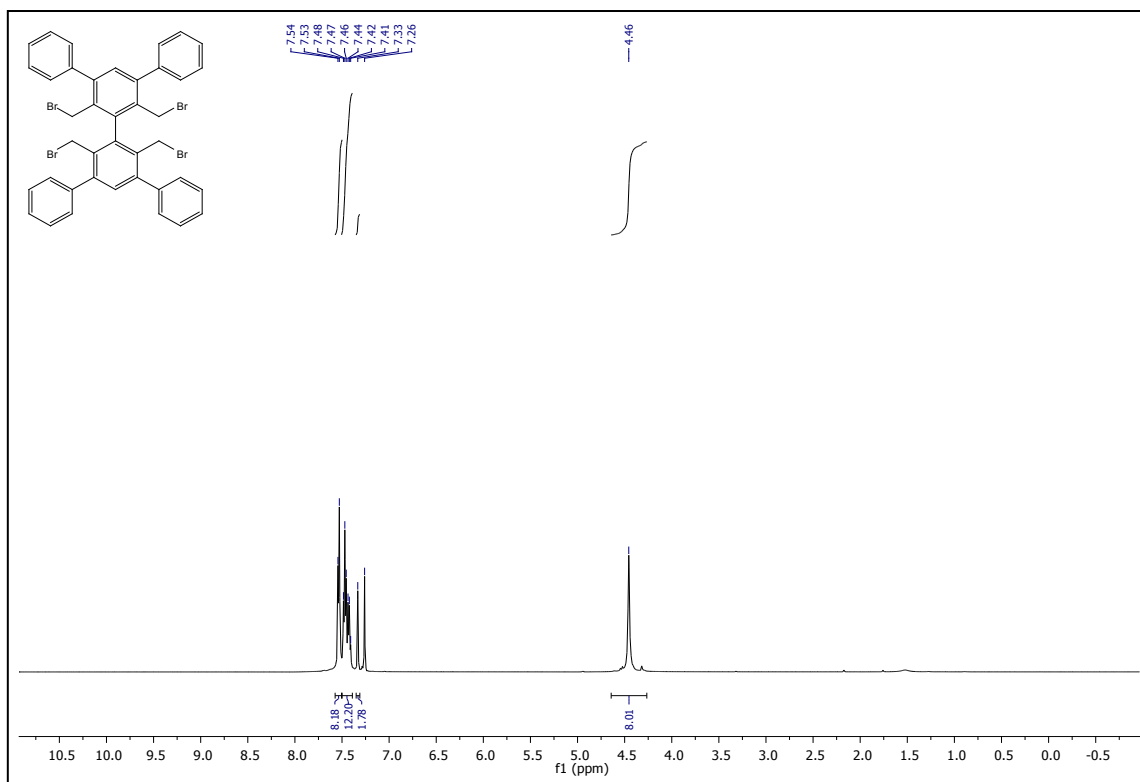


Figure S9. ¹H NMR spectra of **10** at 500 MHz in CDCl₃.

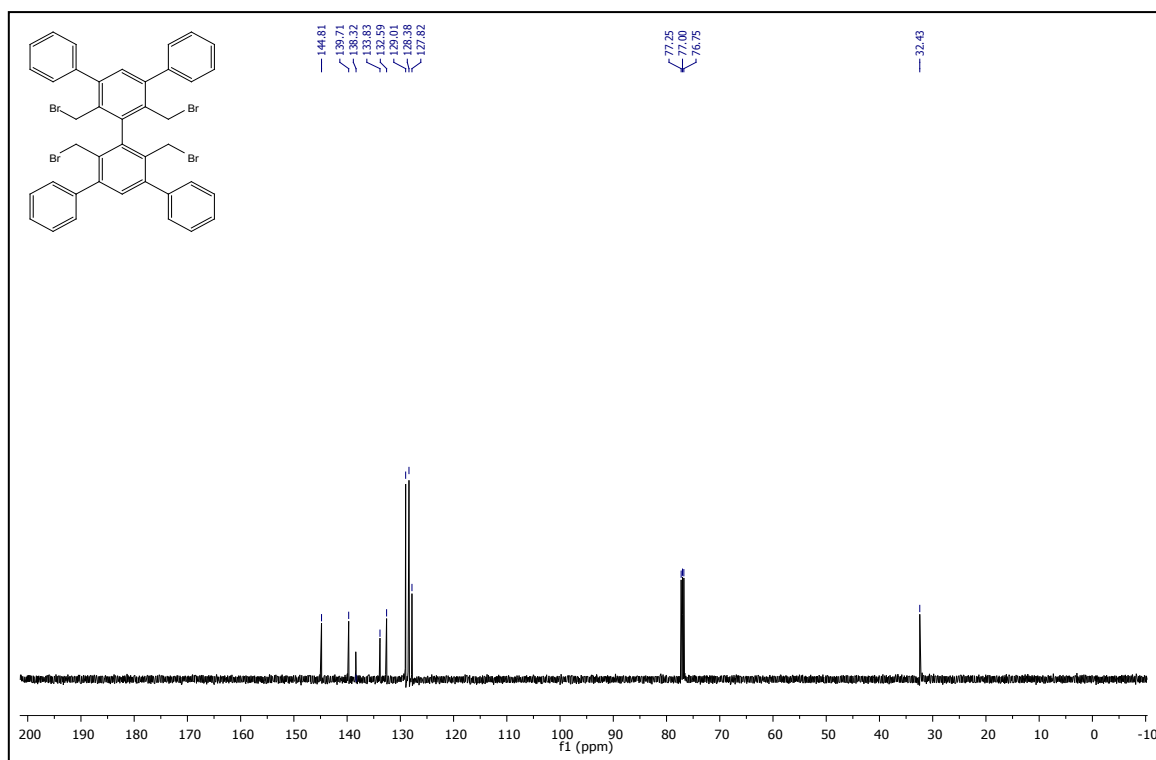


Figure S10. ¹³C NMR spectra of **10** at 125 MHz in CDCl₃.

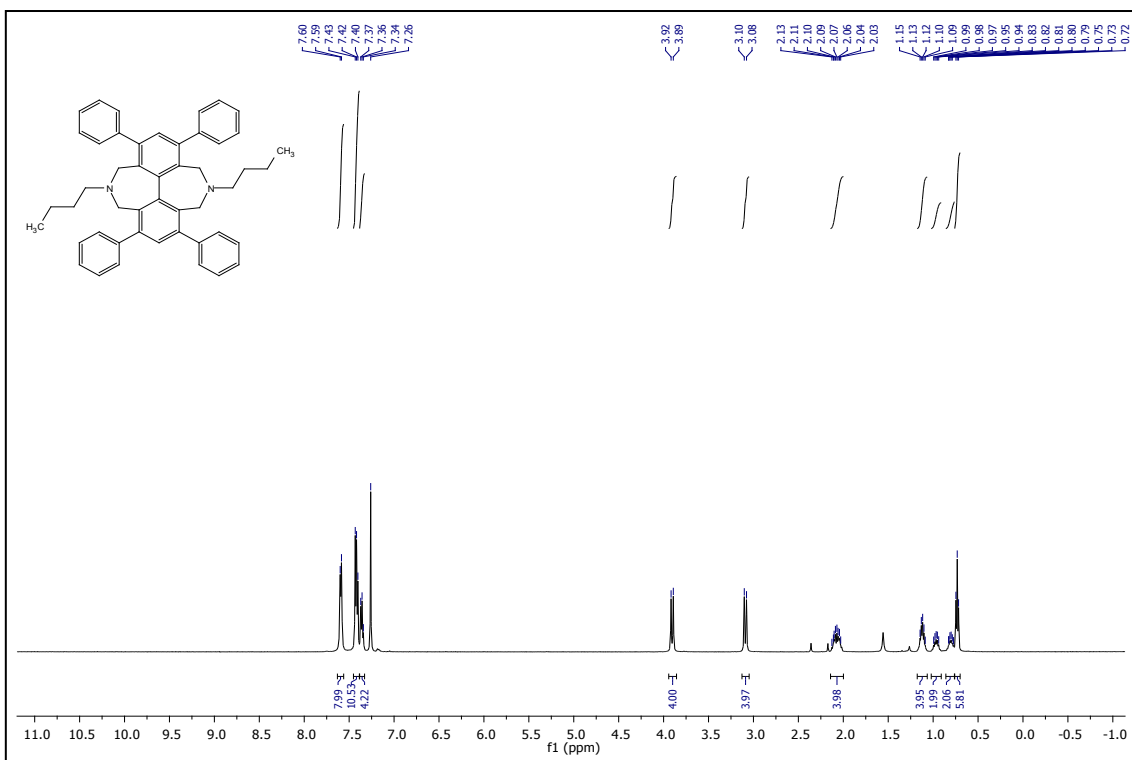


Figure S11. ¹H NMR spectra of **1** at 500 MHz in CDCl₃.

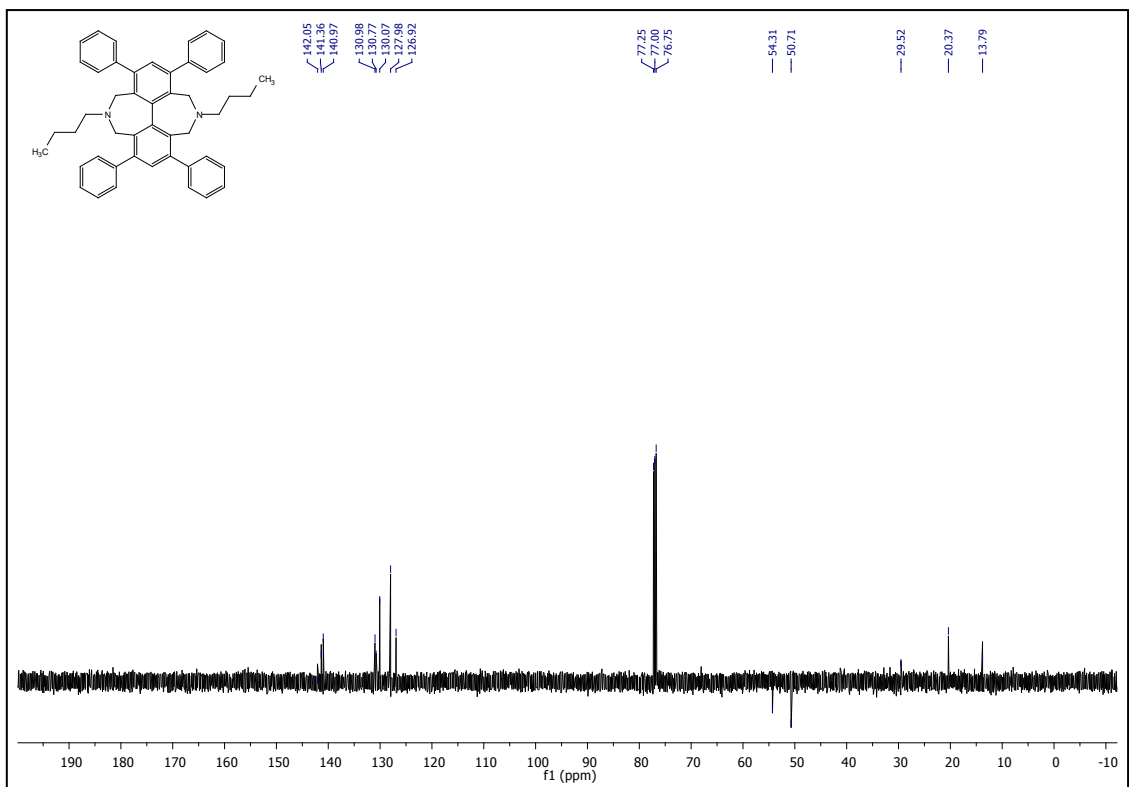


Figure S12. ¹³C NMR spectra of **1** at 125 MHz in CDCl₃.

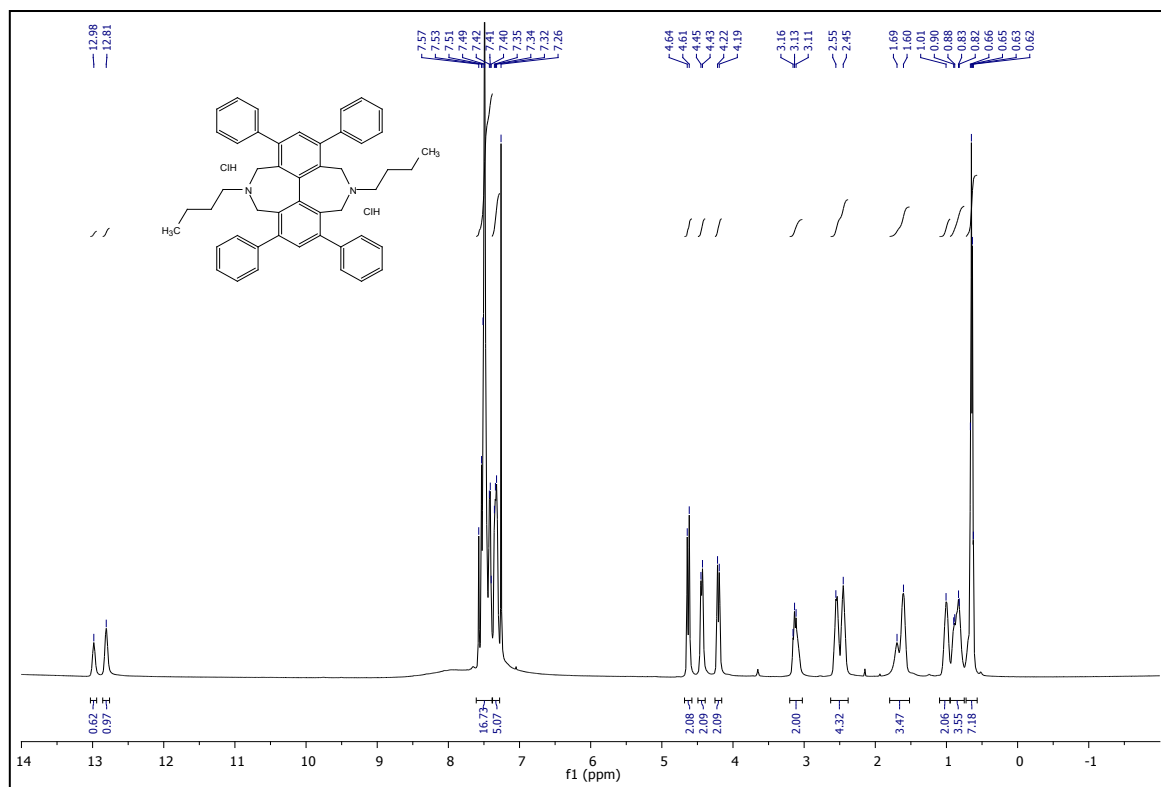


Figure S13. ^1H NMR spectra of **1c** at 500 MHz in CDCl_3 .

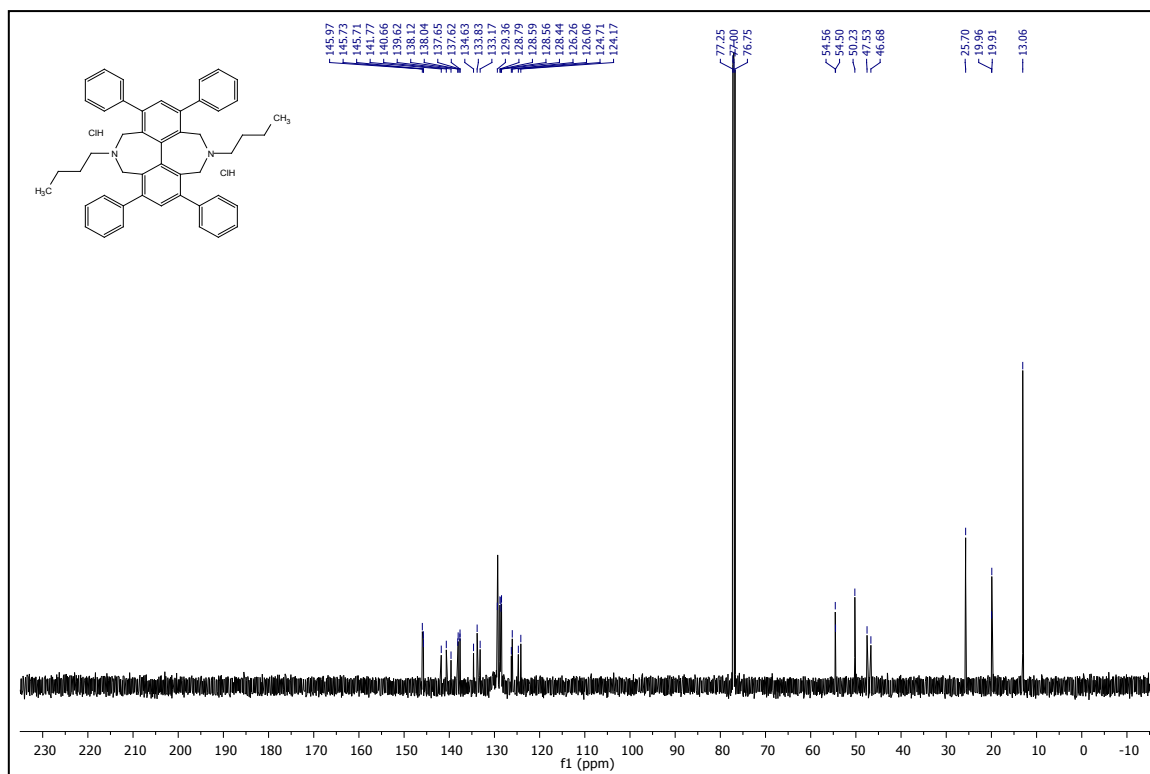


Figure S14. ^{13}C NMR spectra of **1c** at 125 MHz in CDCl_3 .

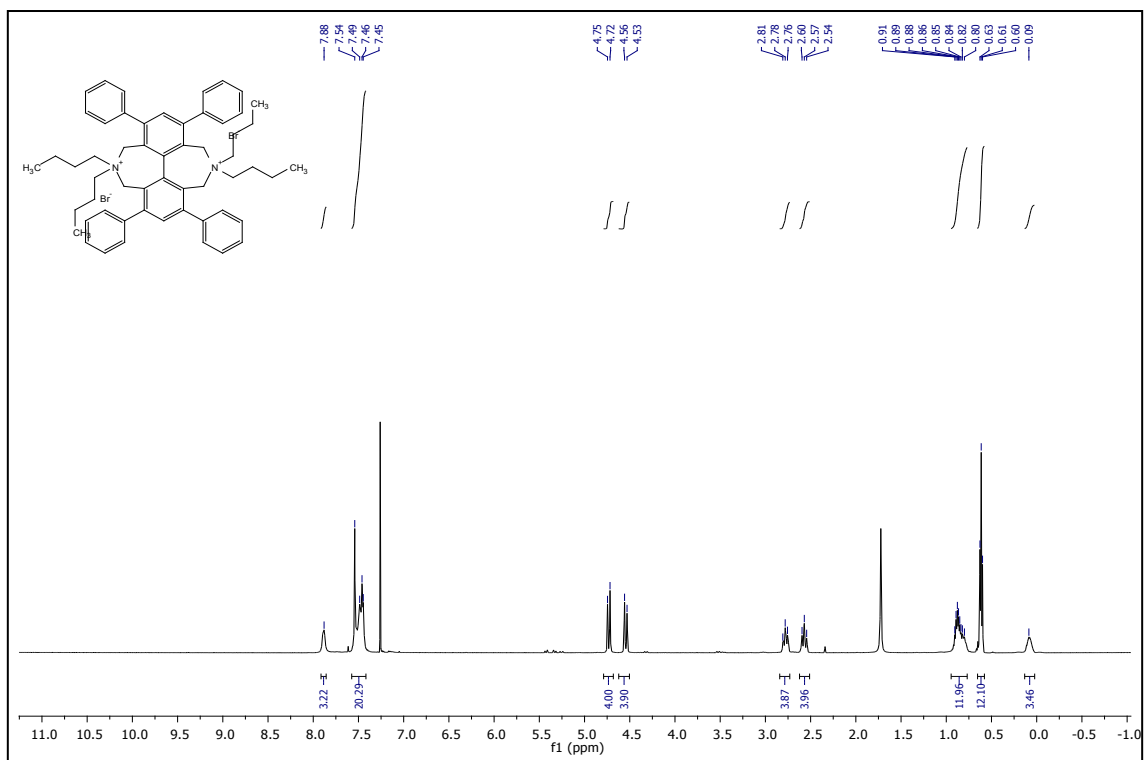


Figure S15. ^1H NMR spectra of **2** at 500 MHz in CDCl_3 .

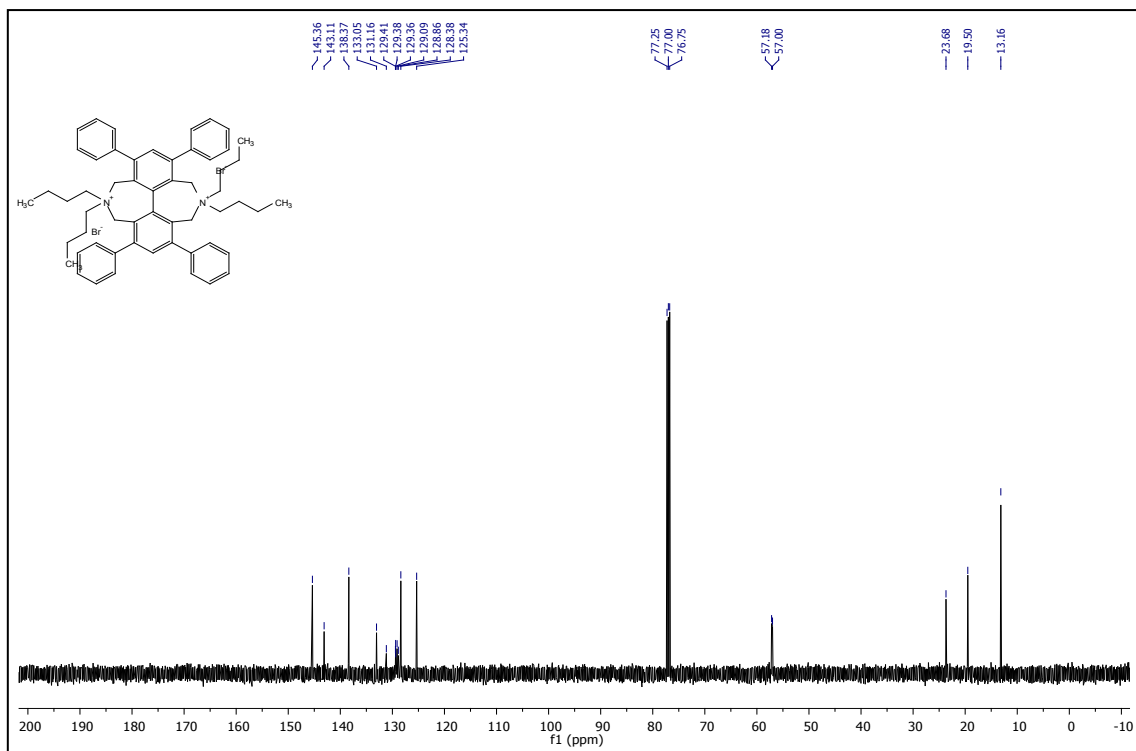


Figure S16. ^{13}C NMR spectra of **2** at 125 MHz in CDCl_3 .

1.3 Growth of the single crystals

The neutral form of compound **1** crystallizes as dimorphs. Form **1a** was obtained from ethanol solution by slow evaporation of the solvent at room temperature. Form **1b** was obtained from dichloromethane solution by slow evaporation of the solvent at room temperature. The chloride salt of **1** (**1c**) crystallized from dichloromethane solution by slow evaporation of the solvent at room temperature. Single crystals of the bromide salt of compound **2** suitable for X-ray diffraction measurements were obtained using three different crystallization techniques. In case of **2a**, **2** was recrystallized from a saturated tetrahydrofuran solution being in equilibrium with the solid powder phase of **2** in a closed ampoule. After a few days diamond shaped crystals appeared in the ampoule, the powder slowly recrystallized into **2a** (Fig. S17). When the solvent from the unsaturated tetrahydrofuran solution of **2** was slowly evaporated, a new polymorphic crystal form of **2b** crystallized (Fig. S18). Using unsaturated tetrahydrofuran/pyridine mixture (5:1) compound **2c** crystallized letting the solvents to evaporate. Crystal structure data are deposited at the Cambridge Crystallographic Data Centre under CCDC 1813220-1813225.

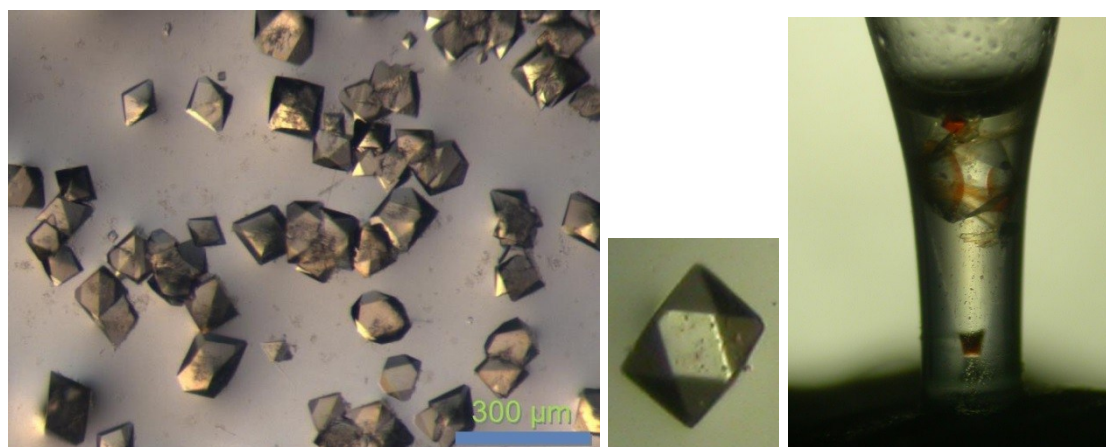


Figure S17 The crystals shape of **2a**.



Figure S18 The Crystal of **2b** after several months.

1.4 Experimental writeup of single crystal structure determination

Intensity data were collected on a Rigaku RAXIS-RAPID II diffractometer (using graphite monochromator; Mo-K α radiation, $\lambda = 0.71075\text{\AA}$) at 113 and 123K in case of crystals **1a-c**, at 293 and 295K in case of crystals **2a-c**, respectively. Low temperature decreased crystal

quality thus available resolution because of cracking. Crystals of **2a-c** were measured in their mother liquor using glass capillary at room temperature. Crystal Clear¹ (developed by Rigaku Company) and SORTAV² (adopted by L. Párkányi) software were used for data collection and refinement. Numerical absorption corrections³ were applied to the data, except **1b** and **1c**, where empirical absorption corrections were used. The structures were solved by direct methods. Anisotropic full-matrix least-squares refinements were performed on F^2 for all non-hydrogen atoms. Hydrogen atoms bonded to C atoms were placed in calculated positions and refined in a riding-model approximation. The computer programs used for the structure solution, refinement and analysis of the structures were Shelx^{4,5}, Sir2014⁶, Wingx⁷, X-Seed⁸ and Platon⁹. In case of framework crystals **2a-c** the channels contain disordered solvent molecules resulting in a continuous electron density which was taken into account by the Squeeze tool of program Platon¹⁰. In the refinement procedure of crystals **1a - 1c** disorder conformations were taken into account. The occupancy of terminal C26' and C26'' atoms was found to be 53 % and 47% in crystal **1a**. The occupancy of terminal C26' and C26'' atoms was found to be 54 % and 46% in crystal **1b**. Crystal **1c**: the occupancy of the disordered terminal butyl C26A, C26B and C26C atoms are 61, 24 and 15%, its neighbouring C25A and C25B are 61 and 39%; One of the phenyl substituent (C17-C18-C19-C20-C21-C22) is disordered over two positions in 59 : 41 ratio, while the other phenyl ring (C11'-C12'-C13'-C14'-C15'-C16') in 54 : 46 ratio. In the calculation of the empty void volumes the void probe radius was set to the value of 1.2 Å in the software Platon. Program Mercury¹¹ and Crystal Explorer^{12,13,14} were used for the graphical representation. Details of crystallographic data, data collection and refinement of crystals **1a-c** and **2a-c** are collected in Table S1.

In case of **1b**, we did not succeed to grow larger crystals than 0.50 x 0.05 x 0.01, the size of the crystals affected the obtained resolution of the diffraction pattern on the R-Axis rapid II diffractometer. In case of the crystals grown from **2**, however the crystal size was sufficient no diffracted rays were obtained at high resolution because of the void system and the disordered tetrahydrofuran molecules in the crystal lattices. In all cases some spots were in shadow of the direct beam catcher at low angle.

The experimental writeup is completed with the text: 'The 3D sponge like crystal structures of **2a-c** are shown in Fig. S33. The crystal lattices contain large channel and void systems. The volume of the voids per unit cell is 6864 Å³ (42%) in **2a** which is theoretically enough for 80

THF molecules (using the approximation that one non-hydrogen atom has a volume of 17.3 Å³). These voids in crystal **2a** were found to be filled with disordered THF molecules resulting in a continuous electron density. The Squeeze tool of Platon was used in space group *P1* with 6864 Å³ void volume in order to remove the unrefinable electron density. The removed 955 electron corresponds to ~24 disorder THF molecules. In this *Fddd* space group, this then implies that the asymmetric unit is associated with 24/32 = 0.75 THF molecules. As the formula unit is composed of 4 asymmetric units this then implies that there are some 3 THF molecules associated with molecule **2** C₅₆H₆₆Br₂N₂.

In crystal **2b**, compound **2** crystallizes in a highly symmetrical space group *Pnna* and the asymmetric unit contains half of the molecule. The void volume per unit cell is lower than in crystal **2a**, it is 2666 Å³ in **2b** which is 39% of the unit cell. Similarly to crystal **2a** the THF molecules were found in disordered positions which were then treated with the Platon Squeeze tool, and 650 electrons were removed representing 16.25 THF molecules. In this *Pnna* space group with *Z* = 4, this then could imply that the formula unit is reported with some 4 THF molecules. The channel system is shown in Fig. S33b. Selected C-H...Br distances and angles are collected in Table S4.

2c crystallised in *P2₁/n* space group and the asymmetric unit contains one molecule of **2** and two pyridine molecules with partial occupation. The void volume is 2398 Å³ (36%) or 1221 Å³ (18%) per unit cell volume depending on the calculation without or with pyridine. The disordered THF molecules were removed by the help of the Squeeze tool of Platon. 290 electrons were removed which refer to about 7 THF molecules. In the *P2₁/n* space group, with *Z* = 4, this then implies that the formula unit is reported with some 1.8 THF molecules. According to the calculated void volume of 1221 Å³, there would have been place for 14 THF molecules. Void system of **2c** is shown in Fig. S33c.

Table S1 Summary of crystallographic data, data collection, structure determination and refinement for crystal **1a-c** and **2a-c**.

Crystal structure	1a	1b	1c	2a	2b	2c
CCDC number	1813222	1813221	1813223	1813224	1813225	1813220
Empirical formula	C ₄₈ H ₄₈ N ₂	C ₄₈ H ₄₈ N ₂	C ₄₈ H ₅₀ Cl ₂ N ₂	C ₅₆ H ₆₆ Br ₂ N ₂ 3 THF	C ₅₆ H ₆₆ Br ₂ N ₂ 4 THF	C ₅₆ H ₆₆ Br ₂ N ₂ ; C ₅ H ₅ N 1.8 THF
Formula weight	652.88	652.88	725.80	1143.23	1215.34	1135.81
<i>F</i> (000)	700	1400	1544	4848	2584	2400
Temperature (K)	103(2)	123(3)	123(2)	293(2)	295(2)	295(2)
Radiation and wavelength	Mo-K α	Mo-K α	Mo-K α	Mo-K α	Mo-K α ,	Mo-K α
Crystal system	triclinic	monoclinic	monoclinic	orthorhombic	orthorhombic	monoclinic
Space group	<i>P</i> -1	<i>P</i> 2 ₁ / <i>n</i>	<i>P</i> 2 ₁ / <i>c</i>	<i>F</i> <i>d d d</i>	<i>P</i> <i>n n a</i>	<i>P</i> 2 ₁ / <i>n</i>
Unit cell dimensions						
<i>a</i> (Å)	12.2542(11)	15.0148(17)	12.4240(8)	22.071(3)	24.343(3)	17.465(3)
<i>b</i> (Å)	12.3204(11)	9.6841(11)	23.0450(15)	25.991(3)	15.987(4)	15.707(3)
<i>c</i> (Å)	12.4610(11)	25.874(3)	15.1970(8)	28.554(4)	17.571(5)	25.981(4)
α (°)	91.981(7)	90	90	90	90	90
β (°)	106.699(7)	100.421(3)	99.050(7)	90	90	110.398(3)
γ (°)	93.107(7)	90	90	90	90	90
V unit cell [Å ³]	1796.9(3)	3700.1(7)	4296.9(4)	16380(4)	6838(3)	6680(2)
V void [Å ³]*	0	80	335	6864 ^a	2666 ^a	2398 / 1221 ^{a,b}
[%]*		2%	8%	42% ^a	39% ^a	36% / 18% ^{a,b}
K.P.I. (%)	68.6	66.4	61.6	41.2 ^a	46.2 ^a	56.7 / 47.5 ^{a,b}
Pore ^c [cm ³ g ⁻¹]	0	0.018	0.069	0.556 ^a	0.433 ^a	0.358 / 0.181 ^{a,b}
<i>Z</i> , <i>Z'</i>	2, 1	4, 1	4, 1	8, 1/4	4, 1/2	4, 1
Density (calculated) (Mg/m ³)	1.207	1.172	1.122	0.927	1.181	1.129
Absorption coefficient, μ (mm ⁻¹)	0.069	0.067	0.184	1.024	1.232	1.255
Crystal colour, description	colourless, platelet	colourless, needle	colourless, block	colourless, chip	colourless, platelet	colourless, chip
Crystal size (mm)	0.50 x 0.50 x 0.10	0.50 x 0.05 x 0.01	0.50 x 0.50 x 0.20	0.58 x 0.55 x 0.45	0.50 x 0.25 x 0.05	0.28 x 0.28 x 0.05
Absorption correction	empirical	numerical	empirical	numerical	numerical	numerical
Min. and max. transmission	0.832 and 1.000	0.969 and 0.995	0.846 and 1.000	0.960 and 0.972	0.974 and 0.996	0.977 and 0.995

θ -range for data collection	$3.120 \leq \theta \leq 25.349^\circ$	$3.113 \leq \theta \leq 21.967^\circ$	$3.081 \leq \theta \leq 25.341^\circ$	$3.135 \leq \theta \leq 20.812^\circ$	$3.045 \leq \theta \leq 21.966^\circ$	$3.087 \leq \theta \leq 20.859^\circ$
	$-14 \leq h \leq 14$;	$-15 \leq h \leq 15$;	$-14 \leq h \leq 14$;	$-22 \leq h \leq 22$;	$-25 \leq h \leq 25$;	$-17 \leq h \leq 17$;
Index ranges	$-14 \leq k \leq 14$;	$-10 \leq k \leq 10$;	$-27 \leq k \leq 27$;	$-25 \leq k \leq 25$;	$-16 \leq k \leq 16$;	$-15 \leq k \leq 15$;
	$-15 \leq l \leq 15$	$-27 \leq l \leq 27$	$-17 \leq l \leq 18$	$-28 \leq l \leq 28$	$-18 \leq l \leq 18$	$-25 \leq l \leq 25$
Reflections collected	27627	32947	70287	30885	26547	6992
Completeness to 2θ	0.998	0.994	0.997	0.996	0.993	0.993
Independent reflections	6561	4488	7826	2139	4151	6992
$R(\text{int})$	0.0551	0.2009	0.0902	0.1380	0.1625	0.2525
Reflections $I > 2\sigma(I)$	4502	2726	5142	879	1864	2979
Data / restraints / parameters	6561 / 0 / 453	4488 / 0 / 463	7826 / 0 / 476	2139 / 0 / 134	4151 / 0 / 274	6992 / 0 / 496
Goodness-of-fit on F^2	1.099	0.978	1.027	1.885	1.043	1.098
Final R indices [$I > 2\sigma(I)$]	$R_1 = 0.0471$, $wR^2 = 0.1044$	$R_1 = 0.0681$, $wR^2 = 0.1306$	$R_1 = 0.0787$, $wR^2 = 0.1945$	$R_1 = 0.2302$, $wR^2 = 0.5471$	$R_1 = 0.1047$, $wR^2 = 0.2801$	$R_1 = 0.1276$, $wR^2 = 0.3386$
R indices (all data)	$R_1 = 0.0777$, $wR^2 = 0.1257$	$R_1 = 0.1207$, $wR^2 = 0.1512$	$R_1 = 0.1205$, $wR^2 = 0.2219$	$R_1 = 0.2968$, $wR^2 = 0.5847$	$R_1 = 0.1862$, $wR^2 = 0.3288$	$R_1 = 0.2138$, $wR^2 = 0.3937$
Max. and mean shift/esd	0.000;0.000	0.000;0.000	0.000;0.000	0.004;0.001	0.000;0.000	0.004;0.001
Largest diff. peak and hole ($\text{e.}\text{\AA}^{-3}$)	0.33;-0.24	0.34 and -0.25	0.51 and -0.51	0.95 and -0.40	0.54 and -0.47	0.82 and -0.58

*Calculated by Squeeze part of the software Platon

^a without THF

^b without pyridine / with pyridine

^c $V_{\text{void}} / (\rho_{\text{calc}}^{\text{b}} \times V_{\text{unit cell}})$

1.5 Generation of Hirshfeld Surfaces

The Hirshfeld surfaces of the investigated molecules in crystals **1a-c** and **2a-c** were calculated by Crystal Explorer 17.5^{12,13,14}. The disordered parts of the diazadibenzo[ef,kl]heptalene derivative molecules were taken into account and high resolution Hirshfeld surfaces were mapped with the functions d_{norm} (normalized contact distance). The Hirshfeld surface of a molecule is generated by points where the contribution to the electron density from the molecule of interest is equal to the contribution from all neighbouring molecules. Each point of this surface has two distances: d_e , the distance from the point to the nearest nucleus external to the surface, and d_i the distance to the nearest nucleus internal to the surface. The combination of d_e and d_i in the form of a 2D fingerprint plots resulted in unique properties of each crystal and provided useful tool to compare intermolecular contacts in different crystals. Hydrogen atom distances were normalised in all calculations of Hirshfeld surfaces (C-H, O-H and N-H distances were 1.083 Å, 0.983 Å and 1.009 Å, respectively). The atomic distances given in tables and figures throughout the paper are calculated based on the single crystal X-ray diffraction measurements.

2. Structure analysis based on single crystal X-ray diffraction

2.1 Discussion of crystal structures of compound 1

The neutral compound **1** crystallized as dimorphs (**1a** $P-1$, and **1b** in $P2_1/n$) and as HCl salt (**1c** in $P2_1/c$). The ORTEP diagrams are shown in Fig. S19. All three structures contain disordered atoms. No framework arrangement can be developed. Comparison of the packing motifs in the different crystals of **1** is shown in Fig. 20.

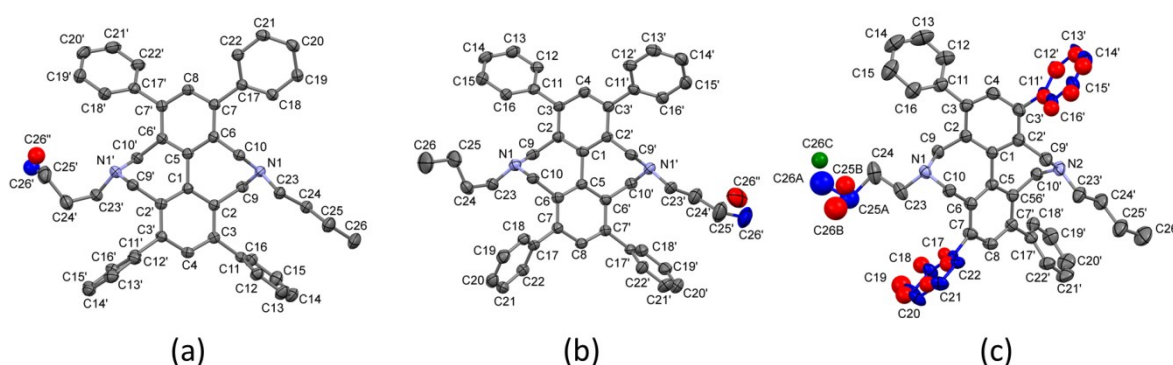


Figure S19. Compound **1**: ORTEP diagrams of the molecules in the crystals of (a) **1a** (b) **1b** and (c) **1c** with displacement ellipsoids presented at 50% probability level. Hydrogens in **1a-1c** and chloride anions in **1c** are omitted for clarity. Disorder atoms are coloured by blue in the major conformer and red in the minor conformer.

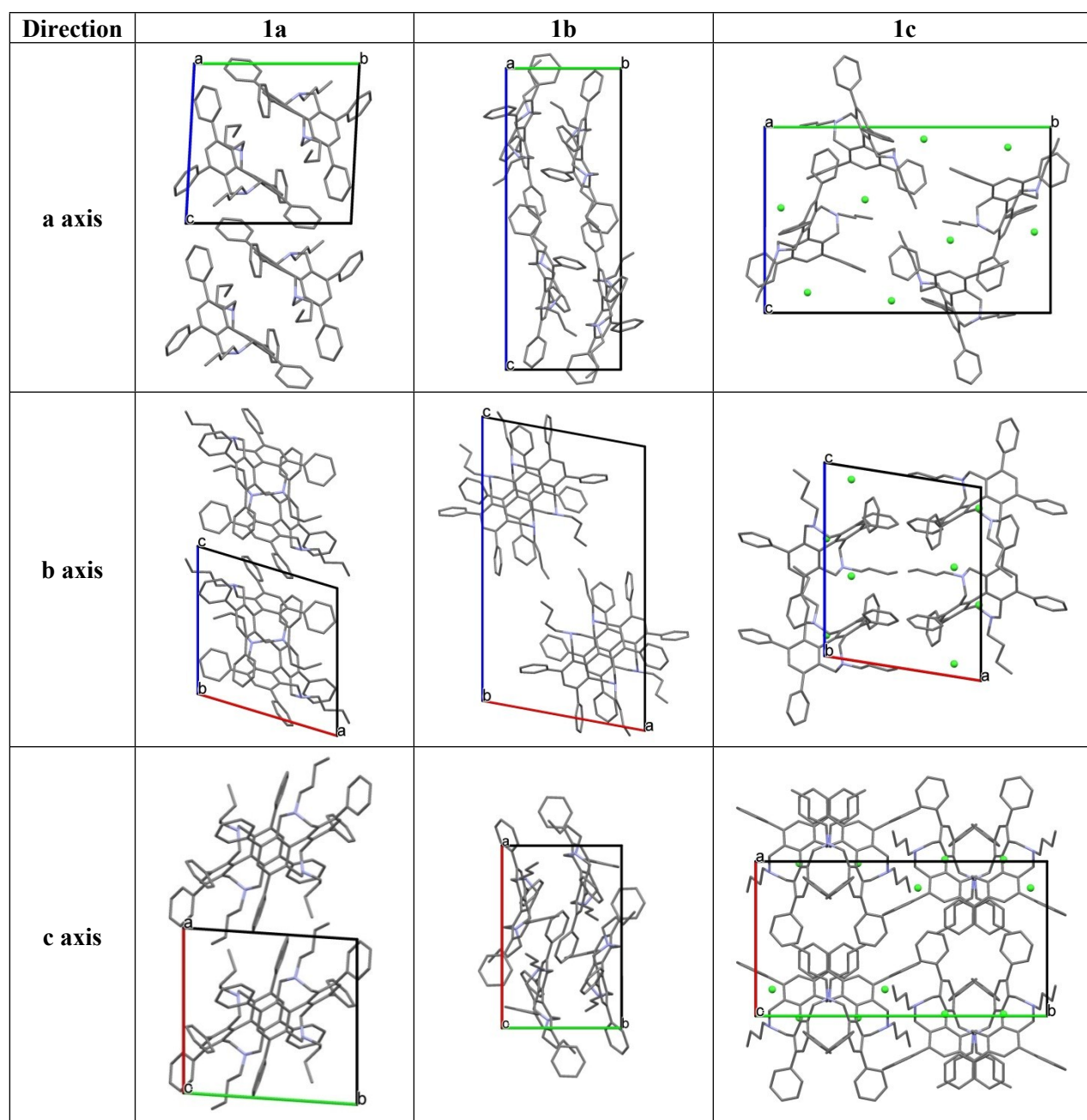


Figure S20. Comparison of the packing motifs in the different crystals of **1**

The arrangement of the molecules in the crystal lattice of **1a** (triclinic, $P-1$, $Z'=1$) are shown from two different crystallographic directions Fig. S21. There is no residual solvent accessible void in the crystal. The packing coefficient (K.P.I=68.6%) is the highest among the reported structures. $C_{\beta\text{ext}}-\text{H}\dots\pi$ intramolecular interactions stabilize the molecular conformation in one half of the molecule, while this interaction does not exist in the other side because of the lack of additional butyl substituents. $\text{C}-\text{H}\dots\pi$ interactions stabilize the crystal structure (Table S2).

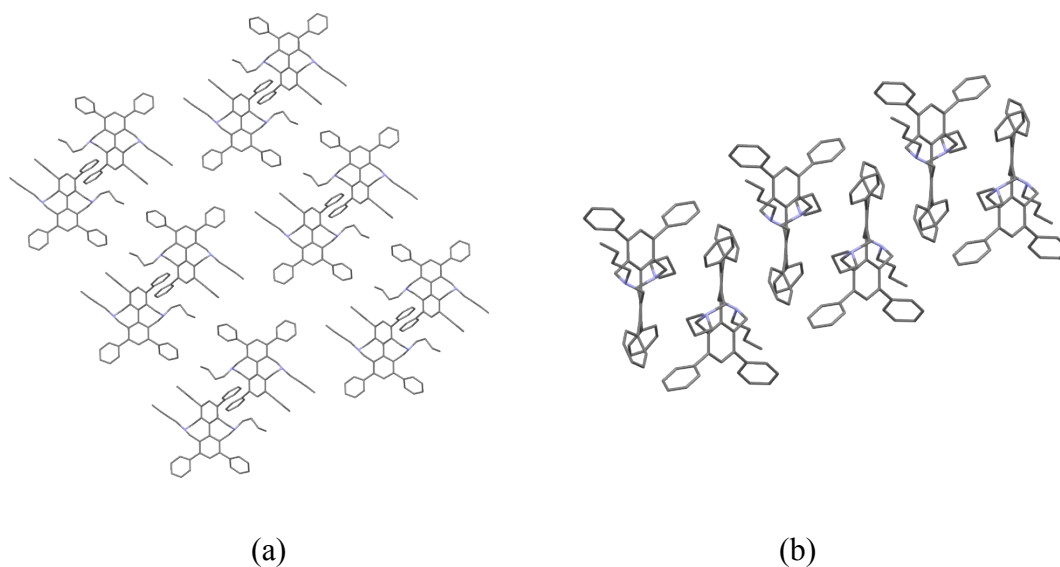


Figure S21. Arrangement of the molecules in crystal **1a** (a) along the diagonal of *ac* axis and (b) along the axis *c*.

1b (monoclinic, $P2_1/n$, $Z'=1$) is shown in Fig. S22. The value of the packing coefficient (K.P.I.=66.4%) shows a closely packed crystal lattice, 2% free space is present in the unit cell. Molecular arrangement is presented in Fig. S22. $C_{\beta\text{ext}}\text{-H}\dots\pi$ intramolecular interactions stabilize the molecular conformation in one half of the molecule, while this interaction does not exist in the other side because of the lack of additional butyl substituents. $\text{C-H}\dots\pi$ interactions stabilize the crystal structure (Table S2).

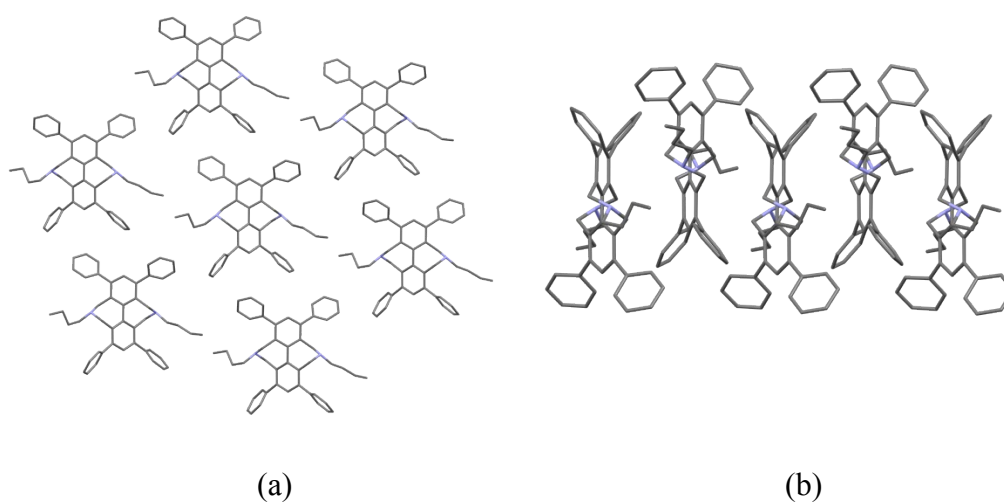


Figure S22. Arrangement of the molecules in crystal **1b** (a) along the *ac* crystallographic plane and (b) along the axis *b*.

Table S2 Intra- and intermolecular C-H... π interactions in the crystal structures of **1a** and **1b**.

	D	H	A (phenyl ring)	D-H [Å]	H...A [Å]	D...A [Å]	D-H...A [°]
1a	C(24)	H(24A)	C(11)-C(12)-C(13)-C(14)-C(15)- C(16)	0.99	2.78	3.652(2)	148
	C(24')	H(24C)	C(11')-C(12')-C(13')-C(14')- C(15')-C(16')	0.99	3.43	4.175(4)	134
	C(9)	H(9B)	C(17)-C(18)-C(19)-C(20)-C(21)- C(22)*	0.99	2.79	3.744(2)	162
1b	C(24)	H(24B)	C(17)-C(18)-C(19)-C(20)-C(21)- C(22)	0.99	3.57	4.345(4)	137
	C(24')	H(24D)	C(17')-C(18')-C(19')-C(20')- C(21')-C(22')	0.99	3.13	3.891(3)	134
	C(19)	H(19)	C(11')-C(12')-C(13')-C(14')- C(15')-C(16')**	0.99	2.88	3.584(5)	132
	C(19')	H(19')	C(11)-C(12)-C(13)-C(14)-C(15)- C(16)***	0.99	2.93	3.613(5)	129

* 1-X,1-Y,2-Z

** 3/2-X,-1/2+Y,1/2-Z

*** 3/2-X,1/2+Y,1/2-Z

In the chloride salt **1c** (monoclinic $P2_1/c$, $Z'=1$) there are small voids, 335 \AA^3 , 8% of the unit cell, that are not large enough to include solvent molecules. The calculated packing coefficient (K.P.I.=61.6%) is less than in **1a** or **1b**. The arrangement of the voids in the unit cell of **1c** is shown in Figure S23. The intermolecular interactions and the packing arrangement of **1c** are shown in Fig. S24 and S25. Selected C-H...Cl and N-H...Cl distances and angles are collected in Table S3. No close C-H... π interaction is present in **1c**.

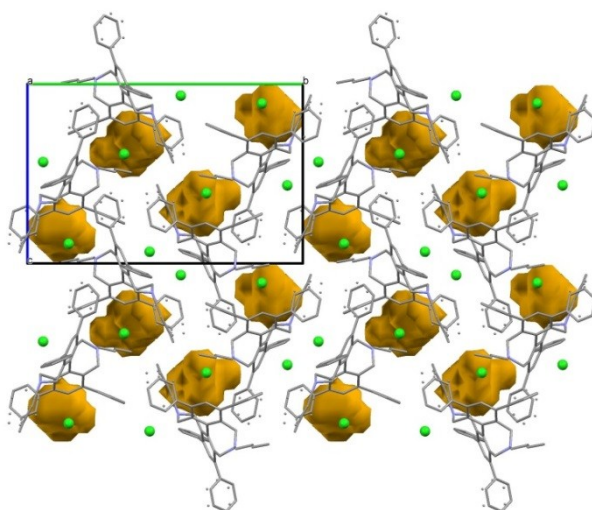


Figure S23. Packing of molecules in crystal **1c** with the indication of voids

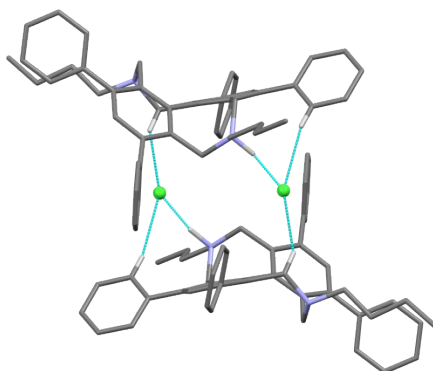


Figure S24. Arrangement of the molecules in crystal **1c** showing the Cl...H contacts between adjacent molecules. Only the major conformer is considered and non-bonded hydrogens are omitted for clarity.

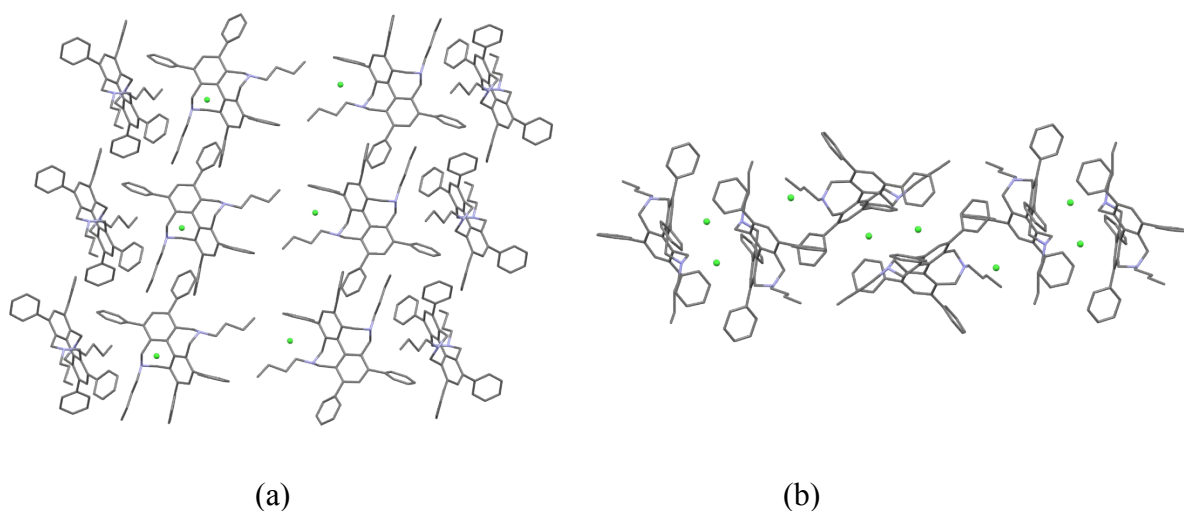


Figure S25. Packing arrangement in crystal **1c** (a) along the *ac* crystallographic plane and (b) along the diagonal of *bc* axis

Table S3 Summary of H...Cl interactions in the crystal lattice of **1c**.

A	H	D	A...H [Å]	A...D [Å]	A...H-D [°]
Cl(1)	H(10A)	C(10)	2.88	3.499(3)	148
Cl(1)	H(10A)*	C(10)*	3.31	3.488(4)	121
Cl(1)	H(9'1)	C(9)	2.61	3.487(5)	92
Cl(1)	H(1N)*	N(1)*	1.90	2.989(3)	164
Cl(2)	H(9A)	C(9)	2.90	3.732(5)	142
Cl(2)	H(23D)	C(23)	2.71	3.516(4)	139
Cl(2)	H(10)**	C(10')**	3.36	3.562(3)	94
Cl(2)	H(2N)**	N(2)**	1.87	2.934(3)	172

Symmetry codes: * $-x, 1-y, 2-z$; ** $x, 1/2-y, 1/2+z$

2.2 Discussion of crystal structures of compound 2

Three different crystal structures have been obtained by various crystallization techniques: the dimorphs from THF (**2a**: orthorhombic, $Fddd$, $Z'=1/4$; **2b**: orthorhombic, $Pnna$, $Z'=1/2$) and their solvatomorph from the mixture of THF and pyridine (**2c**: monoclinic, $P2_1/n$, $Z'=1$;) (Fig. S26).

Conformational symmetry appears having two (**2a**) or one (**2b**) twofold symmetry axes of the molecule. Atoms N1, C1, C4 of **2a** lie on twofold axes. Atoms N1 and N1' of **2b** lie on a twofold axis. The lattice symmetry and the molecular symmetry of the rigid scaffold decrease correspondingly having $1/4$ (**2a**, $Fddd$), $1/2$ (**2b**, $Pnna$) and 1 (**2c**, $P2_1/n$) structural unit in the asymmetric unit of the polymorphs and the solvatomorphic form.

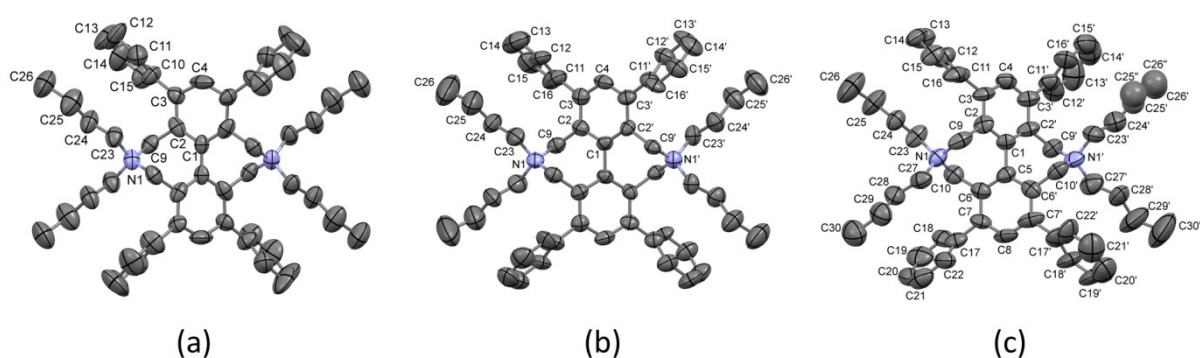


Figure S26. ORTEP diagrams of compound **2** in the crystals of (a) **2a** (b) **2b** and (c) **2c** with displacement ellipsoids at 30% probability level (**2a**) and 50% probability level (**2b** and **2c**). Atoms in the asymmetric unit are labelled according to the Maruoka catalyst. Bromide ions and pyridine molecules in **2c** are omitted for clarity.

The packing arrangement of the three structures (**2a**, **2b** and **2c**) are presented highlighting their similarities (Figs S27, S28 and S29).

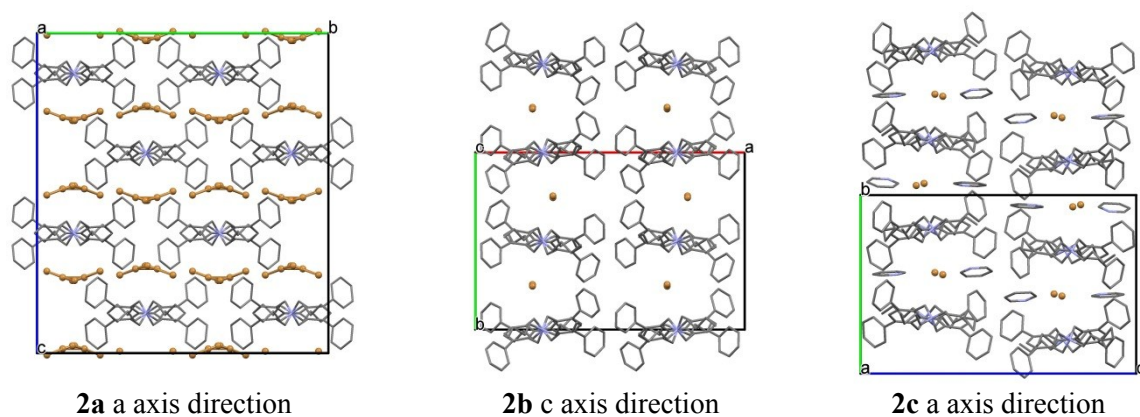


Figure S27. View along the N-N molecular axis

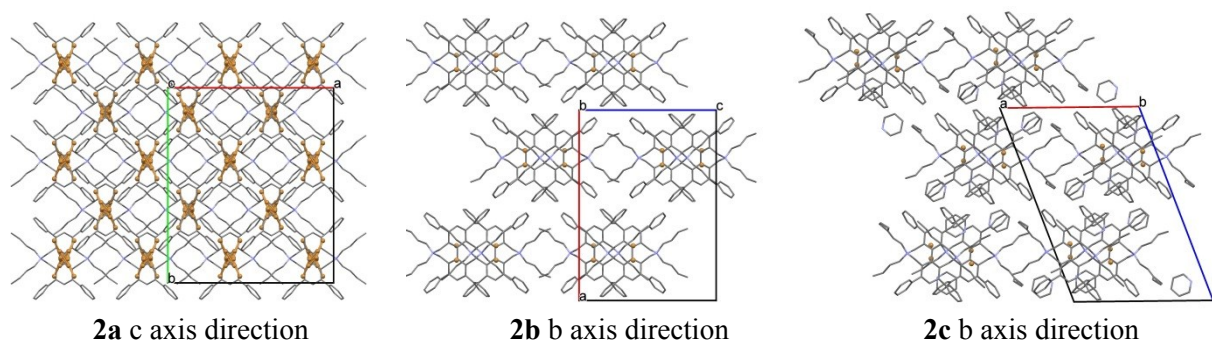


Figure S28. View perpendicular to the plane of the molecules

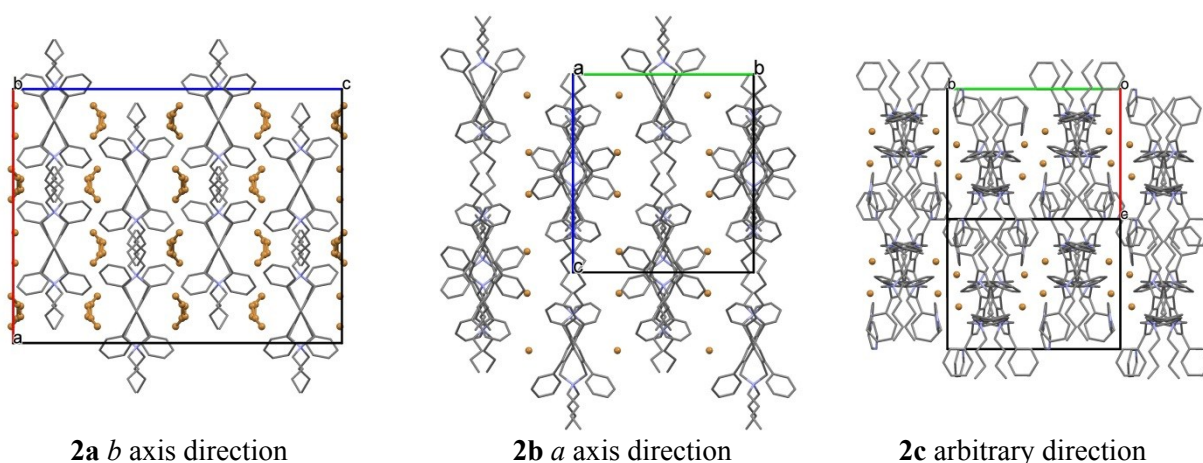


Figure S29. View along the chiral axis of the molecules

The ratio of the butyl and the terminal phenyl groups is 1:1 in compound **2**. $C_{\beta\text{ext}}\text{-H}\dots\pi$ intramolecular interactions (Figure 30, Table S4) between each neighbouring butyl and

terminal phenyl substituent makes the molecule inflexible. Losing the molecular symmetry the lengths of the $C_{\beta\text{ext}}\text{-H}\dots\pi$ interactions slightly vary.

Charge assisted hydrogen bond ($C_{\alpha\text{in}}\text{-H}\dots\text{Br}$) and the recently described $\text{Br}\dots\pi$ interaction between the halide anion and the electron deficient inner phenyl group are responsible for the construction of the framework structure in all three reported crystals **2a**, **2b** and **2c** (Figs. 30, 31 and 32; Table S4).

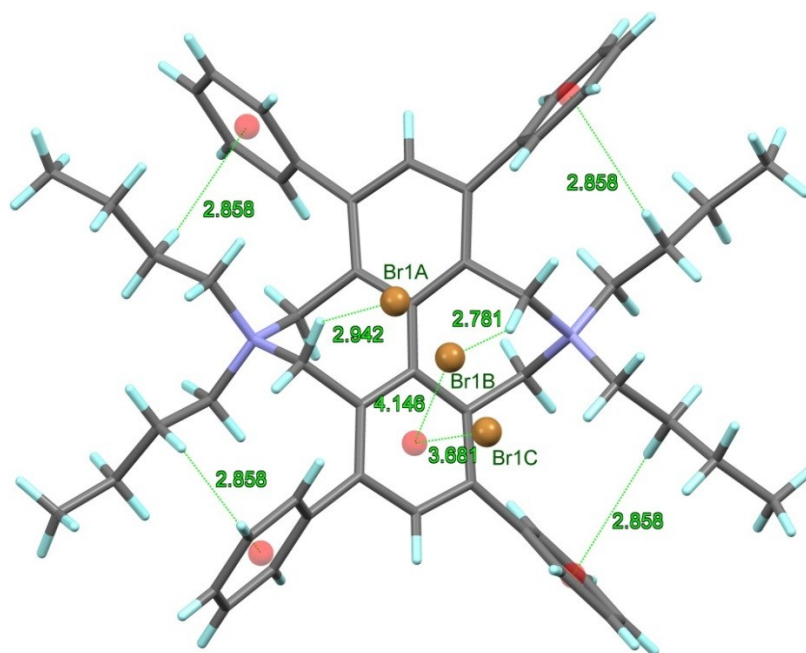


Figure S30. The $C_{\beta\text{ext}}\text{-H}\dots\pi$ intramolecular interactions are responsible for the rigidity of the molecule in the framework structures ($\text{C24-H24A}\dots\pi$) in the example of the structure of **2a**. The $C_{\alpha\text{in}}\text{-H}\dots\text{Br}$ and $\text{Br}\dots\pi$ interactions contribute to the framework architecture ($\text{C9-H9A}\dots\text{Br}$). Br is disordered in **2a** but ordered in **2b** and **2c**.

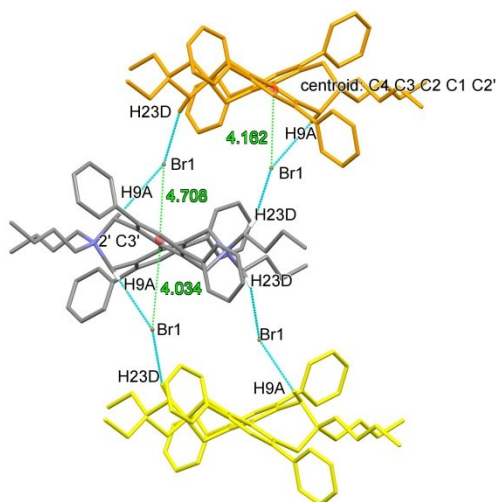


Figure 31. Intermolecular interactions in **2b**.

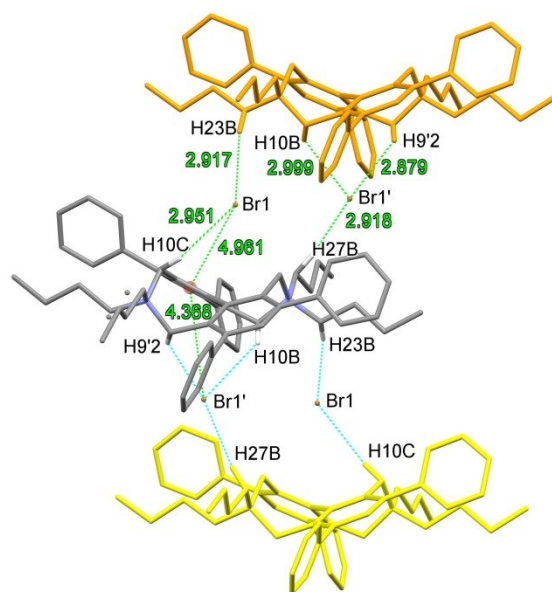


Figure 32. Intermolecular interactions in **2c**.

Table S4 Intra- and intermolecular interactions in the crystal structures of **2a**, **2b** and **2c**.

	A	H	D	A-H dist. (Å)	A-D dist. (Å)	A...H-D ang. (°)
2a	Br(1A)	H(9A)	C(9)	2.96	3.693(15)	133
	Br(1B)	H(9A)	C(9)	2.80	3.675(16)	151
	Br(1B)	H(25A)*	C(25)*	3.07	3.75(3)	149
	Br(1C)	H(9A)**	C(9)**	2.95	3.75(3)	170
	Br(1C)	H(23)***	C(23)***	3.20	4.01(1)	141
	Br(1C)	H(25A)*	C(25)*	2.91	3.75(3)	145
* 1-x,1/4+y,1/4+z ; ** 1-x,-1/4+y,-1/4+z; *** x,1/4-y,1/4-z						
2b	Br(1)	H(9A)	C(9)	2.96	3.729(8)	137
	Br(1)	H(9B')*	C(9')*	3.12	3.675(16)	126
	Br(1)	H(23D)**	C(23')**	2.92	3.857(9)	164
* 1/2-x,-y,z; ** x,1/2-y,3/2-z						
2c	Br(1)	H(9B)*	C(9)*	3.15	3.695(12)	117
	Br(1)	H(10C)*	C(10')*	2.95	3.823(10)	150
	Br(1)	H(23B)	C(23)	2.92	3.848(10)	161
	Br(1')	H(9'2)	C(9')	2.88	3.594(12)	131
	Br(1')	H(10B)	C(10)	3.00	3.706(12)	131
	Br(1')	H(27B)**	C(27)**	2.92	3.868(13)	167
solvent pyridine_1						
	pyridine centre*	H(12)	C(12)	2.79	3.728(8)	157
solvent pyridine_2						
	phenyl ring ^{a,***}	H(1P)_2	C(1P)_2	2.73	3.655(18)	159
* 1/2-x,-1/2+y,1/2-z; ** 1/2-x,-1/2+y,1/2-z; *** 1/2+X,1/2-Y,-1/2+Z						
^a centroid of C(11)- C(12)- C(13)- C(14)- C(15)- C(16) atoms phenyl ring						

The pyridine solvent molecules as neutral linkers take part in the cationic framework construction in the crystal structure of **2c**. C-H... π intermolecular interactions are present between the terminal phenyl groups of the knot molecule and the pyridine linker (Fig. S27 and Table S4).

The tetrahydrofuran is disordered in the large channels in all framework structures. **2a** has very high crystal symmetry (*Fddd*) and the largest volume (42 %) occupied by the disordered solvent molecules. The crystal symmetry (*Pnna* and *P2₁/n*) and the proportion of the voids (39% and 36%) are gradually decreased in **2b** and in **2c**.

The packing images (Fig. S27-S28) demonstrate well the gradual change of symmetry in the arrangement of the molecules in the crystals. The molecules are more and more displaced and the highly symmetric arrangement is distorted. The content of the asymmetric unit increases losing one then another twofold symmetry of the molecule.

The 3D sponge like crystal structures of **2a-c** are shown in Fig. S33. The crystal lattices contain large channel and void systems. The volume of the voids per unit cell is 6864 Å³ (42%) in **2a** which is theoretically enough for 80 THF molecules (using the approximation that one non-hydrogen atom has a volume of 17.3 Å³). These voids in crystal **2a** were found to be filled with disordered THF molecules resulting in a continuous electron density. The Squeeze tool of Platon¹⁰ was used in space group *P1* with 6864 Å³ void volume in order to remove the unrefinable electron density. The removed 955 electron corresponds to 23 disorder THF molecules.

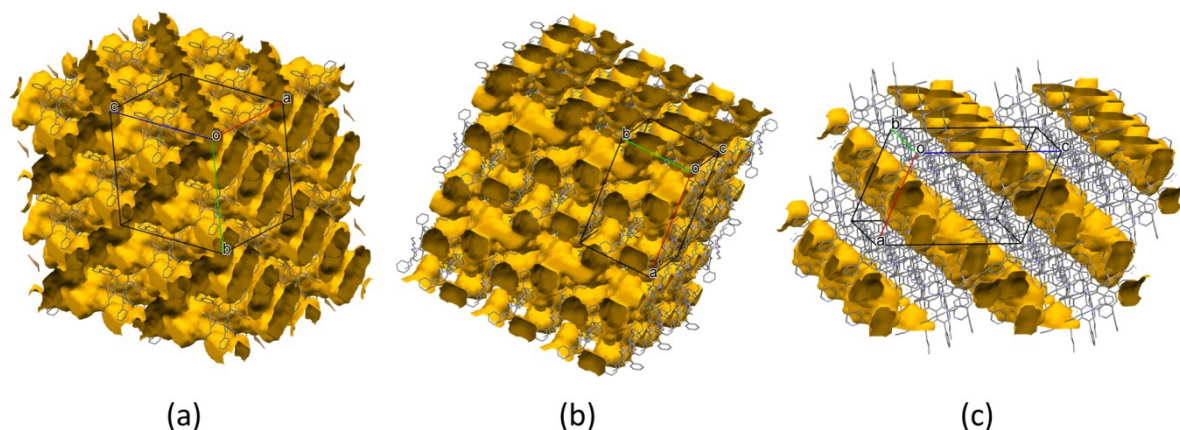


Figure S33. The channel systems (coloured by yellow) of crystals (a) **2a**, (b) **2b** and (c) **2c**.

The bromide ions in **2a** are disordered over parallel and perpendicular passages (irrespective to the channels of the solvent molecules) (Fig. S34).

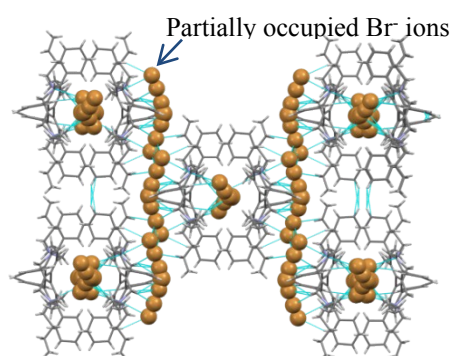


Figure S34. Crystal packing diagrams of **2a** showing the parallel and perpendicular strings of disordered Br ions in the crystal lattice.

In crystal **2b**, compound **2** crystallizes in a highly symmetrical space group *Pnna* and the asymmetric unit contains half of the molecule. The void volume per unit cell is lower than in crystal **2a**, 2666 Å³ which is 39% of the unit cell. Similarly to crystal **2a** the THF molecules were found in disordered positions which were then treated with the Platon Squeeze tool, and

650 electrons were removed representing 16.25 THF molecules. The channel system is shown in Fig. S33b. Selected C-H...Br distances and angles are collected in Table S4.

2c crystallised in $P2_1/n$ space group and the asymmetric unit contains one molecule of **2** and two partially occupied pyridine molecules. The void volume is 2398 Å³ (36%) or 1221 Å³ (18%) per unit cell volume depending on the calculation without or with pyridine. The disordered THF molecules were removed by the help of the Squeeze tool of Platon. 290 electrons were removed which refer to about 7 THF molecules. According to the calculated void volume of 1221 Å³, there would have been place for 14 THF molecules. Void system of **2c** is shown in Fig. S33c.

The crystals of **2a** are loosing THF quickly in air: keeping the crystal shape and transparency the resolution of the diffraction pattern is reduced from 1.0 to 1.6 Å in three days time. **2b** is more durable, stable for some days. Crystals of **2c** are stable in air for a few months. The stability of the crystal increases with the decrease of the void volume.

2.3 Conformational comparison of compound **1** in crystals **1a-c**

The overlay of the molecules from the structures **1a-c** shows high flexibility of the side chains (Fig. S35) The highest maxD and RMSD values (Table S5 and S6) were found between **1c** and **1a**. Comparing the torsion angles, we can see that in one direction of the molecule, namely the line of B, A and C' torsion angles (see Fig. S36), the values are similar, however in the other direction, B',A, C the angles differ considerably. The difference between the conformations is even higher for the butyl side chains. The lack of the second butyl side chain on the nitrogen allow higher flexibility of compound **1** compared to the di-butyl derivative, which results in the rotation of the phenyl groups and in effect in the close packing of the crystals **1a-c**. The higher molecular flexibility results in crystals where the void system is diminished or disappeared. The molecular conformations of the molecular skeletons are very similar for all of the six investigated crystal structures (Table S7).

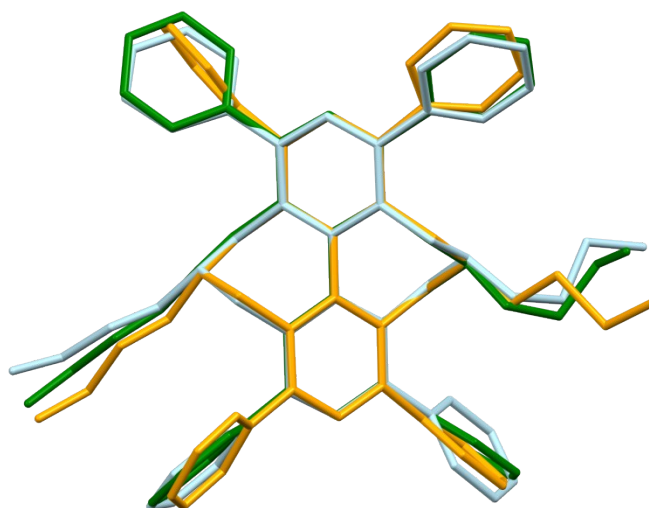


Figure S35. Overlaid structures of **1a** (light blue), **1b** (green) and **1c** (yellow). In case of disordered conformations, the positions with the highest occupancies were used for clarity.

Table S5. Molecular overlay data of the six investigated structures for all heavy atoms (in case of disordered molecular moieties, the molecular conformations with the highest occupancy were considered)

Max.D \ RMSD	RMSD					
	1a	1b	1c	2a	2b	2c
1a		0.5700	0.7855	0.9873	0.9700	0.9598
1b	2.7368		0.9544	0.9775	0.9516	0.9245
1c	1.7878	3.3916		0.6785	0.6977	0.7492
2a	3.5793	3.3406	2.8411		0.1330	0.2070
2b	3.4813	3.0917	2.8467	0.3269		0.1513
2c	3.5187	3.2389	2.9102	0.5861	0.3306	

Table S6. Molecule overlay data of the six investigated structures only for the molecular skeletons

Max.D \ RMSD	RMSD					
	1a	1b	1c	2a	2b	2c
1a		0.0535	0.1019	0.1075	0.0945	0.0839
1b	0.1000		0.0803	0.0829	0.0634	0.0650
1c	0.2328	0.1731		0.0778	0.0628	0.0494
2a	0.2447	0.1486	0.1471		0.0510	0.0735
2b	0.2162	0.1257	0.1458	0.0727		0.0536
2c	0.1843	0.1087	0.0925	0.1364	0.1000	

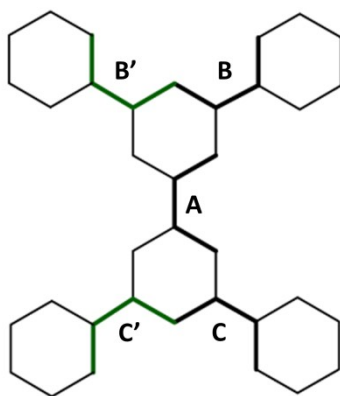


Figure S36. Selected torsion angles used for the conformational comparison

Table S7. Selected torsion angle data (see Fig. S36) of compound **1** in crystals **1a-c** and compound **2** in crystals **2a-c** together with data from Maruoka catalyst

Crystal	A	B	C	B'	C'
1a	49.6(5)	-130.8(4)	-126.0(4)	-135.6(4)	-124.3(4)
1b	47.1(2)	-113.6(2)	-140.13(19)	-93.3(2)	-129.6(2)
1c	51.9(4)	-127.7(4)	-117.3(4)	-112.1(4)	-124.9(4)
2a	52.1(5)	-119.7(9)	-119.7(9)	-119.7(9)	-119.7(9)
2b	52.86(6)	-120.7(10)	-123.6(9)	-120.7(10)	-123.6(9)
2c	50.5(7)	-122.1(6)	-124.9(5)	-120.0(6)	-119.6(7)
MOJGIC^a	58.51	-132.59	-120.56		

^a data of Maruoka catalyst^{15,16}

2.4 Conformational comparison of compound **2** in crystals **2a-c**

The conformation of compound **2** in crystals **2a-c** is highly similar showing inflexibility. The maximum difference (maxD) and root mean square deviation (RMSD) between different structures are collected in Table S5. The highest difference was obtained between structures **2a** and **2c** with the relatively small values of maxD 0.5861 and RMSD 0.2070 (Fig. S37). The identity of conformation is even higher for the centre part of the molecules (Tables S5, S6 and S7).

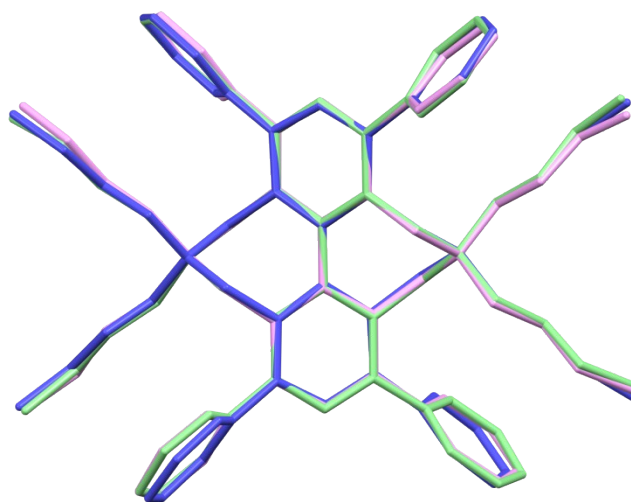


Figure S37. Molecular overlay of **2a** (blue), **2b** (pink) and **2c** (light green)

The similarity of the conformation is further manifested in the torsion angles (Table S8.) however small differences could be obtained especially for the phenyl rings where the large void systems give opportunity for somewhat larger rotational freedom.

Several Maruoka-type catalysts have been synthesized so far^{16,17,18,19} preserving the basic structure but substituting the phenyl rings. In case of DANYIC¹⁸ the substrate was also crystallised together with the catalyst, and found that it is positioned between two catalysts. All of the crystallized Maruoka-catalysts^{16,17,18} have similar conformations in solid phase (Fig. S38 and Table S8), which has a key role in the catalytic reaction. Comparing the Maruoka-catalyst MOJGIC¹⁶ with the structure of **2c** a very good agreement can be seen for the catalytic part of the molecule (Fig. S39).

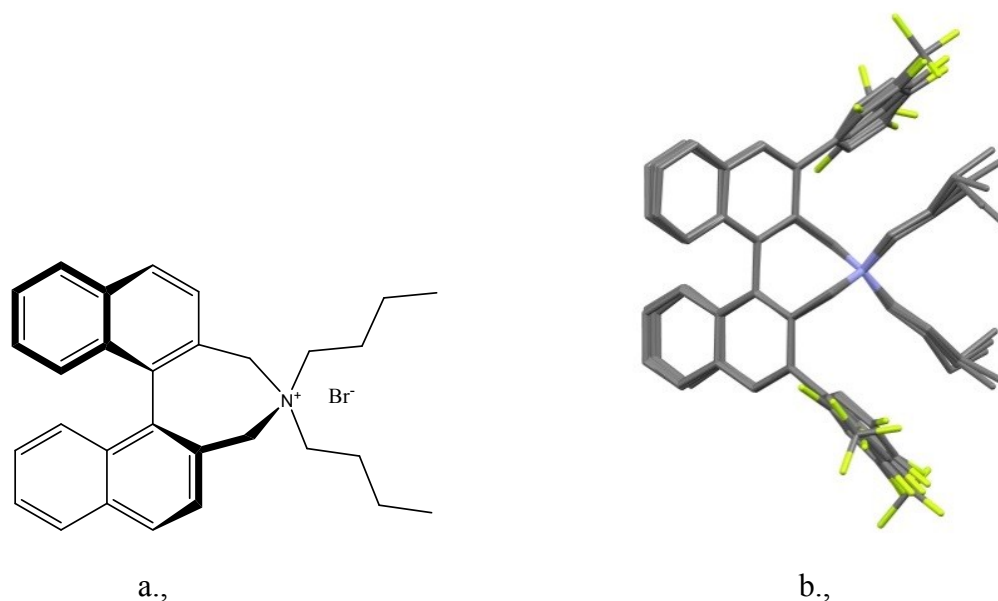


Fig. S38 a., Drawing diagram of the Maruoka type catalyst. b., The Maruoka-catalysts have similar conformation in the crystal lattices^{16,17,18}, the methyl groups in the end of the *n*Bu rotating.

Table S8. The torsion angle of Maruoka catalyst^{16,17,18}.

	Torz 1	Torz 2a	Torz 2b
MOJGIC ¹⁶	58.51	-132.59	-120.56
MOJGOI ¹⁶	57.13	-122.70	-126.18
	54.20	-125.45	-116.56
YAPYAQ ¹⁷	57.37	-112.45	-119.88
MOJGUO ¹⁶	56.34	-103.00	-118.59
DANYIC ¹⁸	56.39	-114.22	-114.22
	62.67	-114.83	-114.83

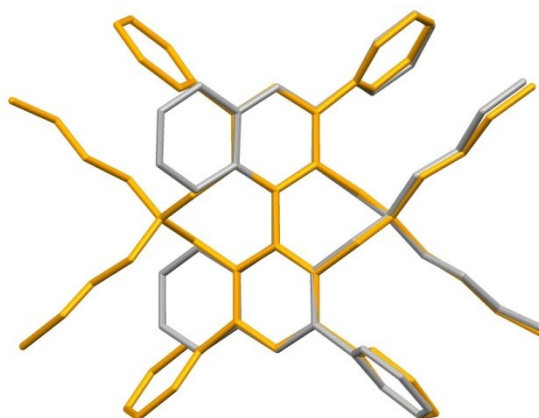


Figure S39. Comparison of the molecular conformations of **2c** (orange) and of the original Maruoka-type catalyst from Ref 16.

3. Intermolecular interactions investigated by Hirshfeld surface analysis

3.1 Hirshfeld surface analysis in structures of compound **1**

In order to investigate the intermolecular interactions and compare them in the different polymorphic crystals Hirshfeld surface analysis was performed. Owing to the flexible n-buthyl side chains in the crystals of compound **1** several atoms were found to be disordered. In case of disordered structures the interpretation of Hirshfeld surface is more difficult. In all cases, the calculation was performed by taking into account the different conformers, resulting in the generation of the Hirshfeld surface based on the electron densities weighted by their partial occupancies. (The conformer with higher occupancy is coloured blue and the one with lower occupancy is red in the figures).

Two types of secondary interactions can be found in the two polymorphous crystals **1a** and **1b**, $H\cdots H$ contacts and $C\cdots H/H\cdots C$ contacts with no considerable spikes on their 2D fingerprint plots (Fig. S40 and Fig. S41). Owing to the flexibility of the molecule, the phenyl rings of adjacent molecules turn in a way to maximize the attractive $C-H\cdots\pi$ interactions (Fig. S40e and S41e). This interaction manifested in the high ratio of $C\cdots H/H\cdots C$ contacts in **1a** and **1b**. Short $H\cdots H$ contacts are measured between a phenyl hydrogen and a buthyl side chain hydrogen atom in **1a** and between two buthyl side chain hydrogens in **1b** (Fig. S40d and S41d).

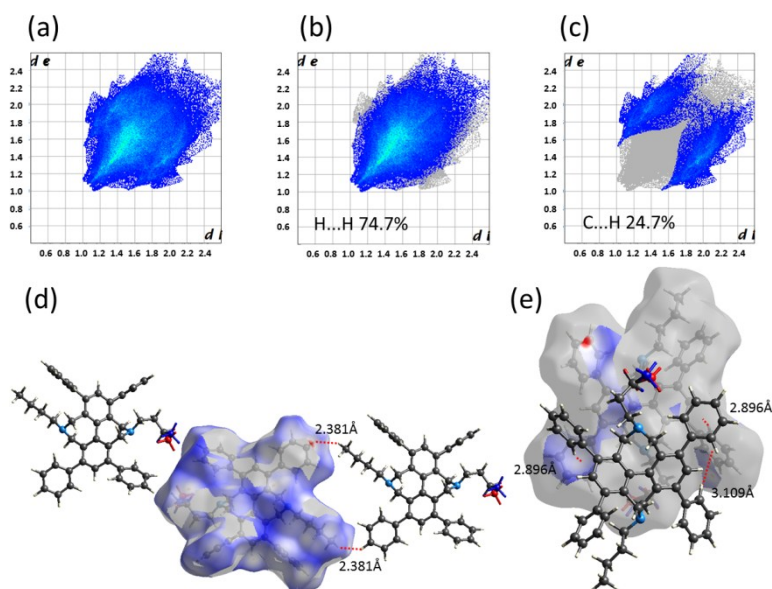


Figure S40. Fingerprint plots and surface maps of compound **1a**. Two dimensional maps showing (a) all the interactions, and highlighting (b) the $H\cdots H$ and (c) the $C\cdots H/H\cdots C$ contacts. (d) Closer $H\cdots H$ contacts. (e) Major $C\cdots H$ contributions from $C-H\cdots\pi$ contacts.

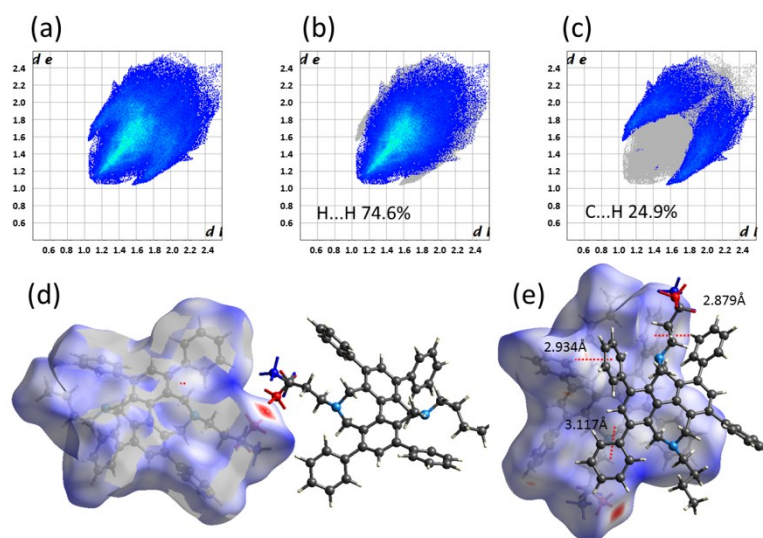


Figure S41. Fingerprint plots and surface maps of compound **1b**. Two dimensional maps showing (a) all the interactions, and highlighting (b) the H \cdots H and (c) the C \cdots H/H \cdots C contacts. (d) Closer H \cdots H contacts. (e) Major C \cdots H contributions from C-H \cdots π contacts.

The more motional freedom was observed in crystal **1c**, two phenyl rings are disordered in two positions, and one n-butyl side chain in three different positions. (In the Hirshfeld surface calculation the two major conformers were considered.) The 2D fingerprint maps and close intermolecular connections in **1c** are shown in Fig. S42. The two chloride counter ions are connected to the protonated nitrogen atoms through hydrogen bonds with short distances (Fig. S42e). The two sharp spikes on the 2D fingerprint plots in Fig. S42c are originated from the very close distance (1.584 Å) calculated between the phenyl ring and butyl chain hydrogens of adjacent molecules (Fig. S42f), however we have to take into account that these groups have two possible orientations and this value comes from the distance when conformer blue and conformer red are chosen. More realistic H \cdots H distances (2.341 Å and 3.252 Å) could be found when the phenyl ring and butyl hydrogens of the same conformers were chosen. In crystal **1c** the H \cdots Cl contacts ensure an attractive interaction and the C \cdots H/H \cdots C contacts have lower contributions (18.8%) to the overall interaction map than those in crystals **1a** and **1b**.

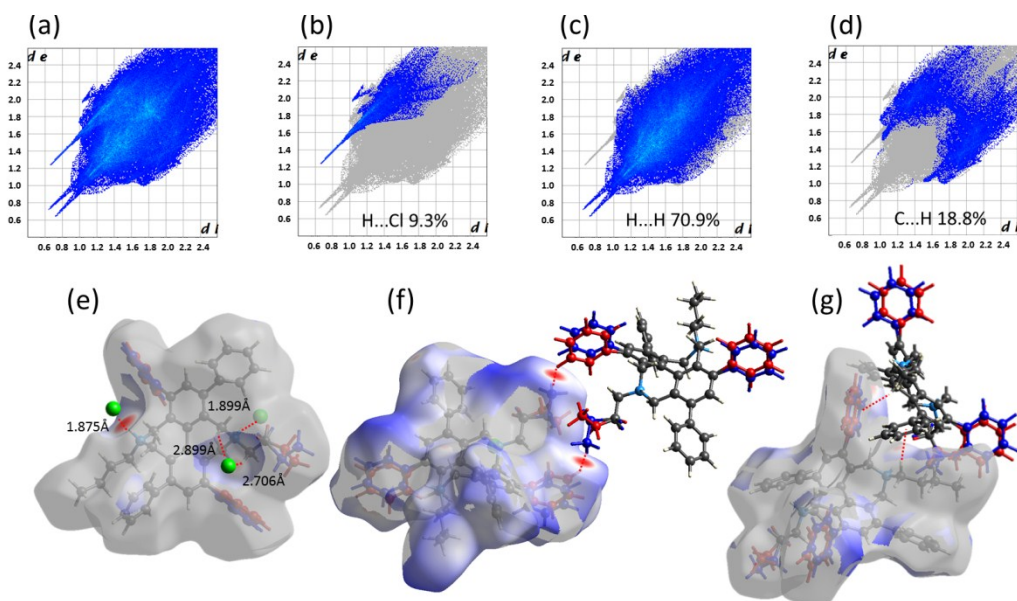


Figure S42. Fingerprint plots and surface maps of compound **1c**. Two dimensional maps showing (a) all the interactions, and highlighting (b) the H \cdots Cl contacts, (c) the H \cdots H and (d) the C \cdots H/H \cdots C contacts. (e) Positions of the two Cl $^-$ ions on the Hirshfeld surface. (f) Shorter H \cdots H contacts. (g) Major C \cdots H contributions from C-H \cdots π contacts.

3.2 Hirshfeld surface analysis for crystals of compound **2**

Because of the extensive void system in crystals **2a-c** containing disordered solvent molecules, only the skeleton of the crystal lattice could be compared, while the contacts between the disordered THF solvents and the host molecules could not be taken into account.

In crystal **2a**, where the amount of void per unit cell was very high, the extension of the Hirshfeld surface can be seen in those directions where the crystal contained voids (Fig. S43). Only a few close contacts appear on the surfaces. The 2D fingerprint plots have been calculated to investigate the contributions of different secondary interactions that are responsible for the different crystal packings observed in the three crystals (Fig. S43). The major interactions are hydrogen-hydrogen contacts (>70 %) between the molecules, in all three cases. The lattices are mainly stabilized by C $_{\alpha}$ -H \cdots Br and C-H \cdots π contacts. In crystal **2a** the 2D plot (Fig. S43) shows that most interaction between molecules are far interactions (most of the contacts are longer than 3 Å). The disordered Br $^-$ ions are placed in a valley generated by the inclined side chains, however closer distances (red spots) can be seen near the C $_{\alpha}$ -H atoms, close to the positively charged quaternary ammonium ion (Fig. 43e). There is a short H \cdots H contact between two phenyl ring hydrogens (C-H13 \cdots H13) with a (non-normalized) distance of 2.121 Å (Fig. S43c and f). The C-H \cdots π contacts give only minor contribution to the overall stabilizing interactions (Fig. S43d).

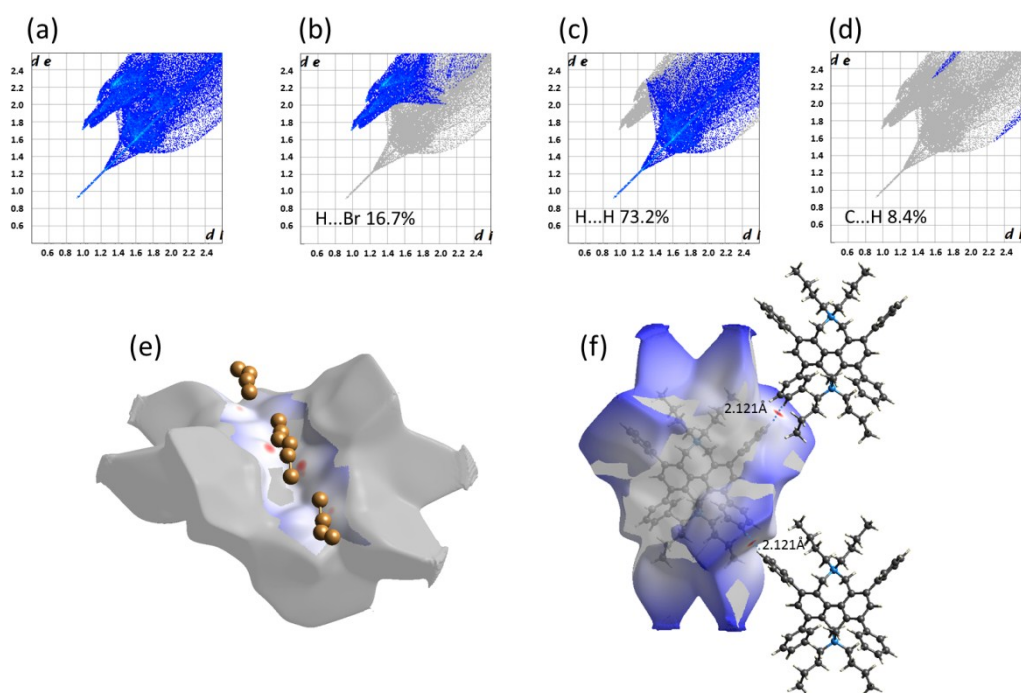


Figure S43. Fingerprint plots and surface maps for compound **2a**. Two dimensional maps showing (a) all the interactions, and highlighting (b) the H \cdots Br contacts, (c) the H \cdots H and (d) the C \cdots H/H \cdots C contacts. (e) Positions of disorder Br⁻ ions on the Hirshfeld surface. (f) Short H \cdots H contacts.

In crystal **2b** the two bromide ions are located close to the quaternary ammonium ion (Fig. S44a), and more tight arrangement of the molecules accomplished. The results of Hirshfeld surface analysis in case of crystal **2b** is depicted in Fig. S44, where the fingerprint plots and the closest H \cdots Br, H \cdots H and C \cdots H contacts are shown. In this crystal the overall contribution of H \cdots Br contacts are found to be somewhat lower (15%) than in **2a** (16.7%), and the two bromide ions are connected to the C $_{\alpha}$ -H hydrogen atoms. The H \cdots H contacts are much more diffuse in the 2D fingerprint plots (Fig. S44c) showing that many H \cdots H contacts appear with similar distances. The closest H \cdots H distance could be measured between a phenyl ring hydrogen and a butyl hydrogen of adjacent molecule in a distance of 2.315 Å (Fig. S44f). The neighbouring molecules turn with their phenyl ring perpendicular to each other which gives possibility to C-H \cdots π contact interactions. The closest hydrogen – ring centroid distance of 3.157 Å could be measured (Fig. S44g).

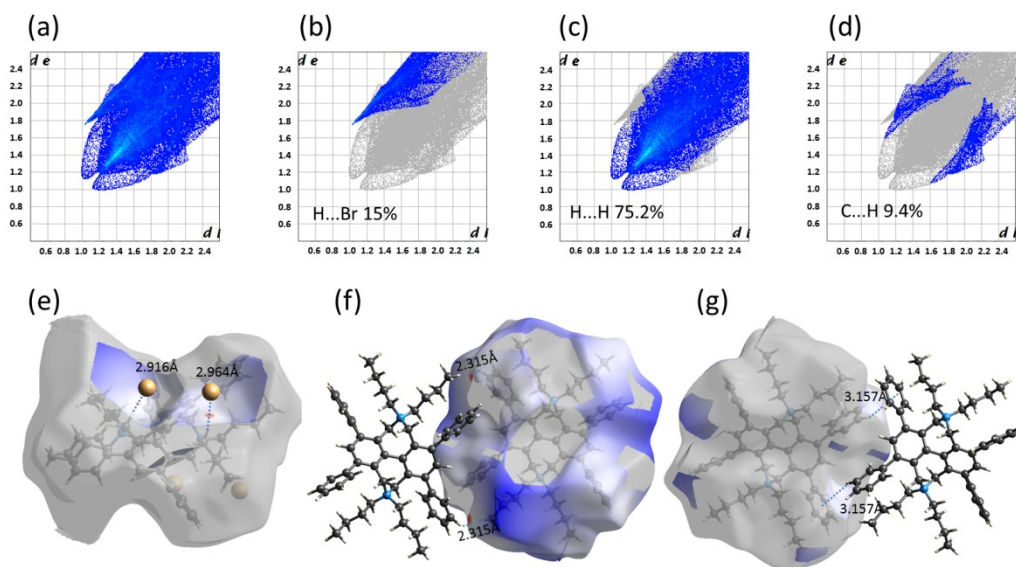


Figure S44. Fingerprint plots and surface maps of compound **2b**. Two dimensional maps showing (a) all the interactions, and highlighting (b) the H \cdots Br contacts, (c) the H \cdots H and (d) the C \cdots H contacts. (e) Positions of the two Br $^-$ ions on the Hirshfeld surface. (f) Closer H \cdots H contacts. (g) Shorter C \cdots H/H \cdots C contributions from C-H \cdots π contacts.

The 2D fingerprint maps and corresponding surfaces of compound **2c** is depicted in Fig. S45. In crystal **2c** the bromide positions and distances from C $_{\alpha}$ -H atoms are similar to **2b**, however the contribution of H \cdots Br contact to the total interactions is significantly less (9.2 %) comparing with 15% in crystal **2b**. This is due to the fact that pyridine molecules also stabilize the crystal structure increasing the ratio of C-H \cdots π interactions, which constitute 13.9% of the overall interactions (Fig. S45d).

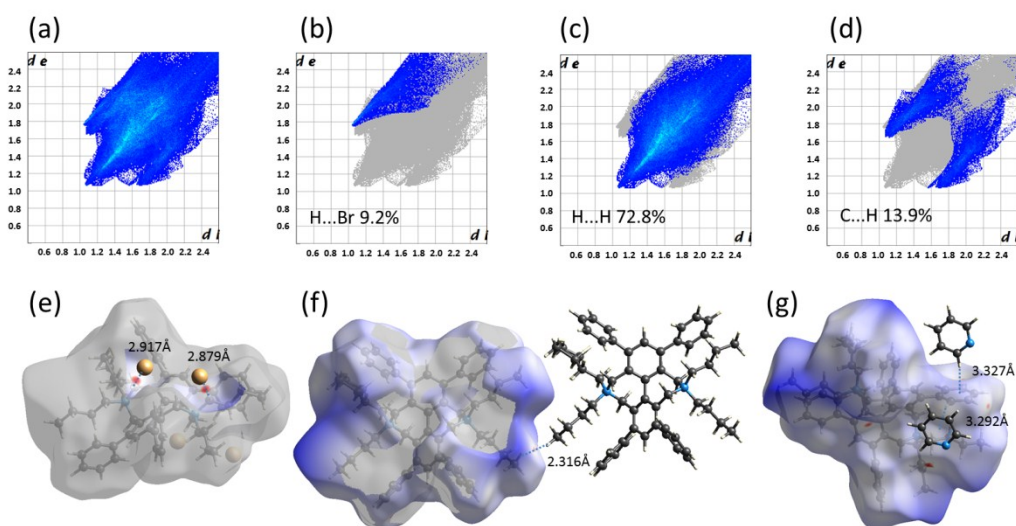


Figure S45. Fingerprint plots and surface maps for compound **2c**. Two dimensional maps showing (a) all the interactions, and highlighting (b) the H \cdots Br contacts, (c) the H \cdots H and (d) the C \cdots H/H \cdots C contacts. (e) Positions of the two Br $^-$ ions on the Hirshfeld surface. (f) Closer H \cdots H contact. (g) Shorter C \cdots H contributions from C-H \cdots π contacts.

The closest H...H distance (2.316 Å) could be measured between two adjacent butyl side chain. The higher amount of C...H interactions is in connection with the increased C-H... π interactions generated between pyridine ring hydrogens and phenyl rings and *vice versa* (Fig. S45g).

Figure S46 summarizes the contribution of all the non-covalent interactions to the crystal stability in each investigated compound. We can conclude that the ratio of the halogen-hydrogen interaction is higher in **2a** and **2b** than in **2c**. The C...H (C-H... π) contact is more pronounced in crystal **2c**, when pyridine is present than in **2a** or **2b**. In case of compound **1**, the higher flexibility of the molecule allows the phenyl rings to rotate to form more C-H... π interactions.

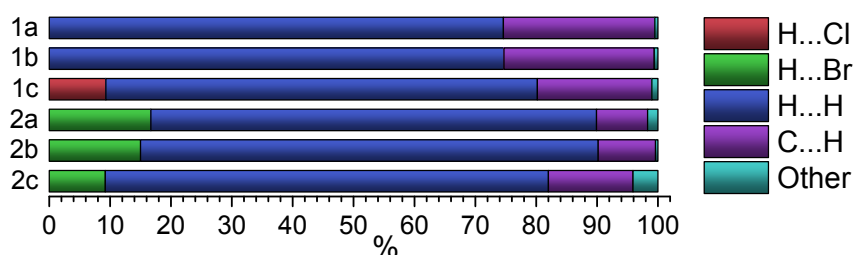


Figure S46. Relative contribution of the various intermolecular contacts to the Hirshfeld surface area in crystals **1a-c** and **2a-c**.

References

- CrystalClear SM 1.4.0 Rigaku/MSI Inc., 2008.
- R. H. Blessing, *Acta Cryst.*, 1995, **A51**, 33-38.
- NUMABS: Higashi, T. (1998), rev. 2002. (Rigaku/MSI Inc.)
- G. M. Sheldrick, *Acta Cryst.* 2008, **A64**, 112-122.
- G. M. Sheldrick, *Acta Cryst.* 2015, **C71**, 3-8.
- M. C. Burla, R. Caliandro, B. Carrozzini, G. L. Casciarano, C. Cuocci, C. Giacovazzo, M. Mallamo, A. Mazzone and G. Polidori, *J. Appl. Crystallogr.*, 2015, **48**, 306-309
- L. J. Farrugia, *J. Appl. Crystallogr.*, 2012, **45**, 849-854.
- L. J. Barbour, *Journal of Supramolecular Chemistry*, 2001, **1**, 189-191.
- A. L. Spek, *Acta Cryst.* 2009, **D65**, 148.
- A.L. Spek, *Acta Crystallogr C Struct Chem.* 2015, **71**, 9-18.
- C. F. Macrae, P. R. Edgington, P. McCabe, E. Pidcock, G. P. Shields, R. Taylor, M. Towler, J. van de Streek, *J. Appl. Cryst.* 2006, **39**, 453-457.
- M.A. Spackman, D. Jayatilaka, *CrystEngComm*, 2009, **11**, 19-32.
- M.A. Spackman, J.J. McKinnon, *CrystEngComm*, 2002, **4**, 378-392.
- J.J. McKinnon, M.A. Spackman, A.S. Mitchell, *Acta Cryst. B*, 2004, **60**, 627-668.
- I. J. Bruno, J. C. Cole, P. R. Edgington, M. Kessler, C. F. Macrae, P. McCabe, J. Pearson, R. Taylor, *Acta Cryst.*, 2002, **B58**, 389-397.

16. Kitamura, M.; Shirakawa, S.; Arimura, Y.; Wang, Xisheng; Maruoka K. *Chem.Asian J.*, 2008, **3**, 1702-1714.
17. Kitamura, M.; Shirakawa, S.; Maruoka K. *Angew.Chem.,Int.Ed.* 2005, **44**, 1549-1551.
18. Shirakawa, S.; Liu, Kun; Maruoka, K. *J.Am.Chem.Soc.* 2012, **134**, 916-919.
19. K. Maruoka, *Organic Process Research and Development* 2008, **12**, 679-697.